Seismic Wave Propagation in Thinly-Layered Media with Steep Reflectors

H. Lydia Deng

— Master of Science Thesis —

Center for Wave Phenomena
Colorado School of Mines
Golden, Colorado 80401
(303) 273-3557

ABSTRACT

Seismic waves reflected from steep reflectors in the earth's subsurface spend a significant amount of time travelling more or less horizontally. Therefore, accurate imaging of steep geologic structure requires knowledge of the behavior of these horizontally propagating waves. In particular, the effect of *tunneling* on seismic waves propagating in thinly-layered media must be understood.

I describe a method for modeling seismic waves traveling in thinly-layered media. This method, a frequency-wavenumber finite-difference scheme coupled with the Born approximation, is useful in studying seismic waves reflected from steep geologic structures.

For thinly-layered media, reflected seismic waves show frequency-dependent amplitude and phase behavior that varies with the reflection dip. This dip-dependent attenuation and dispersion is not well understood and is ignored in conventional seismic processing.

Waves propagating vertically in a sequence of thin layers are known generally to lose high frequencies by *stratigraphic filtering*. However, waves reflected from steep reflectors in a thinly-layered medium are additionally attenuated and dispersed by the less well-known *evanescent filtering*. Seismic waves become evanescent when they arrive at a high-velocity layer at post-critical angle. When the high-velocity layer is thin relative to a seismic wavelength, a significant amount of low-frequency energy *tunnels* through to an adjacent lower-velocity layer. Repeated tunneling, as a result of alternating high- and low-velocity layers, yields attenuation and dispersion of seismic waves reflected from steep reflectors. An improved understanding of this filtering action may help us to improve seismic processing techniques used to image steep geologic structures.

i

INTRODUCTION

Overview

Studies of acoustic well logs show that a major portion of the stratigraphic column of the Gulf of Mexico is made up of a binary sequence of alternating layers of sand and shale (e.g., Velzeboer, 1981). It is also common to find massive salt structures in that area. Only recently, seismologists have begun to directly image steep geologic structures in the Gulf, such as overhanging salt domes intruding into a sequence of thin sedimentary layers. While reflection seismic data can give a good indication of the presence of salt, accurate imaging of the flanks of salt bodies requires both a good understanding of seismic waves in thinly-layered media and adequate processing techniques (Larner et al., 1989).

Seismic waves reflected from nearly vertical interfaces, such as the flanks of salt domes, spend a significant amount of time traveling more or less horizontally. These horizontally traveling waves behave differently from the well-understood vertically traveling waves, especially in thinly-layered media. This behavior difference is typically ignored in seismic data processing. A good understanding of the behavior of horizontal traveling waves may help us to improve our processing of seismic reflections from steep interfaces.

The purpose of this research is to study the behavior of seismic waves propagating in thinly-layered media, in particular, waves that are reflected from steep interfaces. A qualitative understanding of this behavior is obtained by analyzing the frequency-dependent attenuation of seismic waves reflected from dipping interfaces.

Modeling techniques based on a high-frequency, WKBJ approximation cannot properly represent seismic waves traveling in thinly-layered media. The study of seismic waves traveling in such media requires a different modeling approach. In this thesis, a modeling algorithm is described that generates synthetic zero-offset surface seismograms in earth models consisting of thin sedimentary layers and steep geologic structures.

Observations of synthetic seismograms show that seismic waves traveling in thinly-layered media are attenuated and dispersed differently for different interface dips. This dip-dependent wavelet shaping is related to the difference of propagation angles of seismic waves propagating in a sequence of sedimentary layers. *Stratigraphic filtering* (e.g., O'Doherty and Anstey, 1971; Banik et al., 1985a; Banik et al., 1985b; White et al., 1990) caused by destructive interference of short-period multiples, is well known to attenuate high frequencies of the seismic signal. Waves traveling in a sequence of thin sedimentary layers may also lose their high frequencies through *evanescent filtering*, because only the low-frequency energy *tunnels* through thin, high-velocity layers (e.g., Fuchs et al., 1976). Attenuation of seismic waves reflected from steep interfaces in thinly-layered media may likely be attributed to both stratigraphic and evanescent filtering.
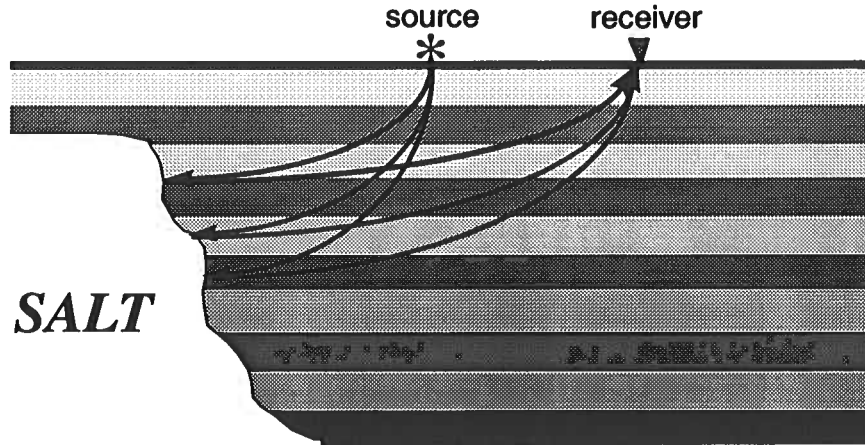
FIG. 1. Seismic waves reflected from a steep interface spend a significant amount of time traveling more or less horizontally in an increasing-trend, velocity-layered medium.

Background

In a stack of sedimentary layers, elastic wave speeds alternate with depth because of lithologic variations, but the velocities usually also tend to increase with depth. In this thesis, I refer to such a medium as *increasing-trend, velocity-layered* medium. If the spatial wavelength (i.e., dominant thickness of layers) of the medium is comparable to or smaller than the wavelength of the seismic signal, the layers of the medium are considered to be thin.

Figure 1 shows such a geologic model. Because the velocity of the medium has an increasing trend with depth, seismic rays taking off from the Earth's surface exhibit increasing propagation angles (i.e., angles as measured with respect to the vertical) with increasing depth. At some depth, some of the rays travel horizontally along sedimentary layers before being reflected from an overhanging interface. Therefore, seismic waves reflected from steep interfaces spend a significant amount of time traveling nearly horizontally.

When seismic waves arrive at a high-velocity layer with their incident angle larger than the critical angle, the propagating waves become *evanescent*. Since amplitudes of these evanescent waves decay exponentially away from the layer boundary, they are typically ignored in seismic data processing. However, if the thickness of the high-velocity layer is small relative to the wavelength of the seismic signal, the evanescent waves behave differently from the evanescent phenomenon with which we are familiar. The amplitude decay with distance of long-wavelength evanescent waves is slower than that of short-wavelength waves. When evanescent waves arrive at the boundary
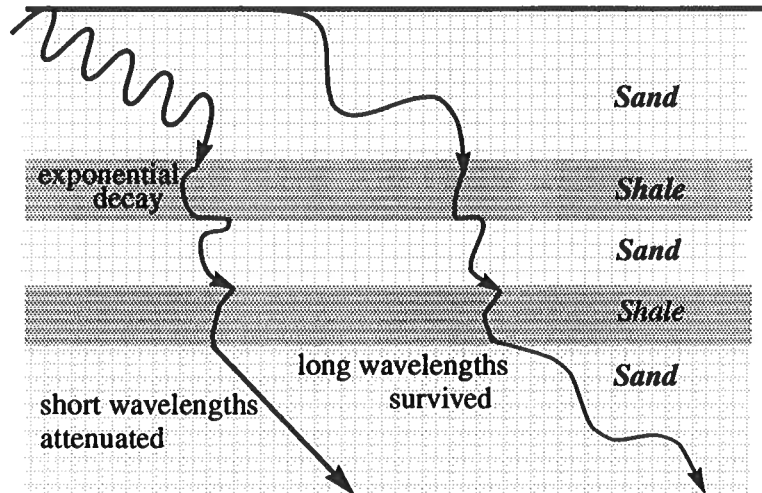
FIG. 2. Seismic waves become evanescent when they reach the boundary of a high-velocity layer beyond post-critical angle. In the high-velocity layer, the amplitudes of high-frequency components decay faster than those of low-frequency components. Some of the low frequencies tunnel through the high-velocity layer while high frequencies do not.

of a low-velocity layer before their amplitudes exponentially decay to negligible values within the high-velocity layer, the transmitted waves become propagating again. These long wavelength waves are known as *tunnel* waves; they have *tunnelled* through the thin, high-velocity layer.

Repeated tunneling attenuates the high-frequency content of seismic waves that travel through a sequence of alternating layers with large propagation angles. Figure 2 schematically illustrates the frequency-dependence of this evanescent filtering.

Investigations

Conventional ray theory is based on a *high-frequency* assumption. That is, the dominant wavelength of seismic waves is assumed to be short relative to the dominant spatial length scale, such as the thickness of layers or the distance between the source and the receiver (e.g., Bleistein et al., 1984). The validity of this assumption can be measured by a dimensionless factor, a/λ, where a is the dominant spatial length and λ is the dominant wavelength of the signal. The high-frequency assumption is valid only if

$$a/\lambda \gg 1.$$

However, the media we are interested in are those for which the thicknesses of layers are comparable to, or even smaller than, the typical wavelength of the seismic signal. For such media, the high-frequency assumption in ray theory may fail to accurately predict even the first-arrival times. A "full-wave" method must be used to accurately describe waves propagating in thinly-layered media.

To reduce the complexity of dealing with both dipping geologic structures and thinly-layered sedimentary media, the modeling used in this research is performed in two steps:

1. Calculate the Green function for a sequence of thin sedimentary layers, ignoring the existence of geologic structure. A *frequency-wavenumber finite-difference* (FKFD) scheme is used to compute this Green function.

2. Using the Green function, compute reflections from dipping interfaces via the *Born approximation.*

The well-known reflectivity method (e.g., Aki et al., 1980) is commonly used to model seismic waves propagating in layered media. However, this method is valid only for homogeneous layers. For a medium where velocity continuously changes, perhaps linearly with depth, the many thin homogeneous layers required to represent this medium make the reflectivity method prohibitively expensive, because each interface between the layers must be dealt with individually. A finite-difference method is preferred under this circumstance because its computational cost is practically independent of the complexity of velocity and density functions of depth. I have implemented Korn's (1988) frequency-wavenumber, finite-difference method, which takes advantage of the lateral homogeneity of the medium and computes the Green function due to a line or point source at any depth.

Given the computed Green function, reflections from a steep interface are computed via a first-order Born approximation. The first-order approximation is valid as long as reflection coefficients of interfaces are small enough (i.e., $r < 5\%$) (Bleistein et al., 1985).

The error caused by numerical approximation in this modeling technique is insignificant in the study of the amplitude and phase behavior relevant to this research. Since the computational cost of generating synthetic seismograms is independent of both the complexity of the velocity and density function and the complexity of the shape of the interface, this algorithm is a relatively efficient method to model seismic waves propagating in thinly-layered media with complex geologic structure.

With this modeling algorithm, we can generate synthetic seismograms and study the behavior of seismic waves traveling in thinly-layered media, specifically, seismic waves reflected from steep interfaces.

Seismic waves that travel vertically through a sequence of thin layers are known to lose their higher frequencies. O'Doherty and Anstey (1971) first observed and

4

analyzed the frequency-dependent attenuation due to short-period multiples which is known as *stratigraphic filtering*. The filtering action is similar to the attenuation within inelastic media, though these two phenomena result from totally different mechanisms. Further investigations of stratigraphic filtering (e.g., Banik et al., 1985; White et al., 1990) have led to a quantitative understanding of the attenuation of waves traveling in a thinly-layered medium.

However, this study of the frequency-dependent attenuation was based on the assumption of a 1-D model, i.e., seismic waves traveling vertically through layered media . When seismic waves propagate into a sequence of thin layers at other angles, their amplitudes and phases can be affected by evanescent filtering as well.

Figure 3 shows frequency spectra of modeled seismic reflections from vertical and horizontal interfaces embedded in an increasing-trend, velocity-layered medium. The thickness of the layers is 150 m, comparable to the wavelength of the acoustic signal. Waves reflected from the vertical interface are more bandlimited than those reflected from the horizontal interface. The main difference between the two spectra is the loss of high-frequency energy in the reflection from the vertical interface.
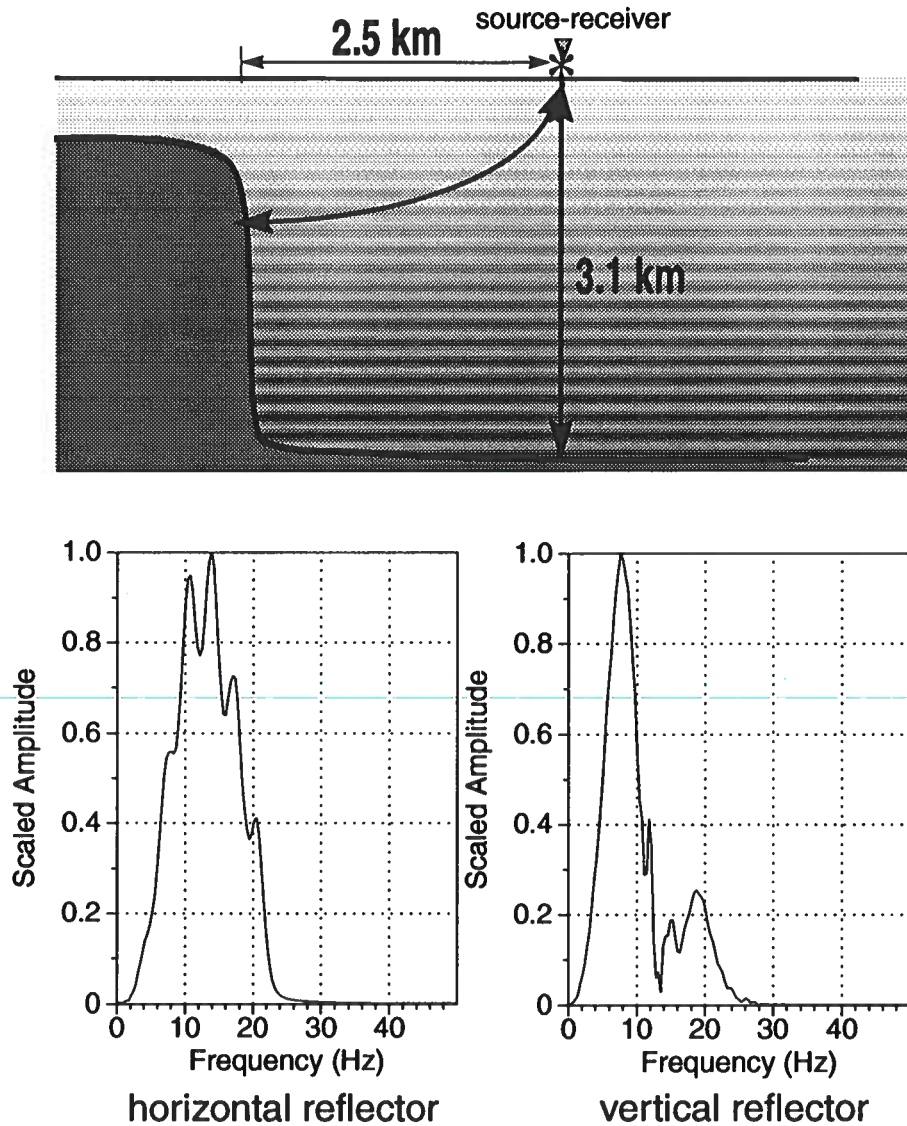
FIG. 3. The upper figure depicts the velocity model and acquisition configuration used to generate seismograms throughout this thesis. The bottom two graphs show the scaled frequency spectra of the reflections from a horizontal and vertical interface embedded in a sequence of thin layers. The velocity of the medium has a linear trend of $1.6 + 0.5\,z$ (km/s) and a sinusoidal variation with a spatial wavelength of 150 m. The source signal has a dominant frequency of 10 Hz.

MODELING OF SEISMIC WAVES IN THINLY-LAYERED MEDIA

Conventional modeling methods, based on the WKBJ approximation, are invalid for layered media that have spatial wavelengths comparable to, or thinner than, the seismic wavelength; the high-frequency assumption on which the WKBJ approximation depends is not satisfied. Hence, a "full wave" method must be used to model seismic waves propagating in thinly-layered media.

The modeling used in this research is performed in two steps. First, compute the Green function in a sequence of sedimentary layers using the *frequency-wavenumber finite-difference* (FKFD) modeling algorithm of Korn (1987), ignoring the existence of the interface. Then, using the Green function, compute waves reflected from an interface embedded in the sedimentary layers via the *Born approximation* (Bleistein 1985). This two-step modeling algorithm separates the complexity of dealing with steeply dipping geologic structures from that of dealing with sedimentary bedding.

Here, I describe this modeling algorithm and discuss its accuracy.

Green's Function

A large variety of methods for modeling seismic wavefields in vertically inhomogeneous media has been developed. Each method has its particular advantages and disadvantages. Due to high-frequency assumptions, conventional methods based on the WKBJ approximation fail to predict even the first arrival times for waves traveling in *thinly* layered media. Commonly used reflectivity methods become prohibitively expensive for media where the velocity is continuously changing, or media that contain many thin layers. The basic assumption for reflectivity methods is that the medium is made up of homogeneous layers, and interfaces of each layers must be dealt with individually. The FKFD algorithm introduced by Korn (1988) has no high-frequency approximation, and the seismic wavefield is computed for all depths simultaneously.

The FKFD algorithm is a combination of integral transformations and a finite-difference technique. The wavefield for each frequency and wavenumber, the *frequency-wavenumber response* of the medium, is calculated by a one-dimensional finite-difference scheme. The summation of these frequency-wavenumber responses yields the seismic wavefield in the medium.

Finite-differencing in depth enables the algorithm to handle complicated velocity and density variations with depth, the computational cost depending mainly on the bandwidth of seismic signals rather than on the complexity of velocity and density functions. Evaluation of the wavefield at an arbitrary depth in the medium requires no additional computation, as the wavefield is calculated simultaneously for all depths.

A Frequency-Wavenumber, Finite-Difference Algorithm

The acoustic wave equation may be reduced to a second-order ordinary differential equation when the wavefield is decomposed for each frequency (ω) and wavenumber
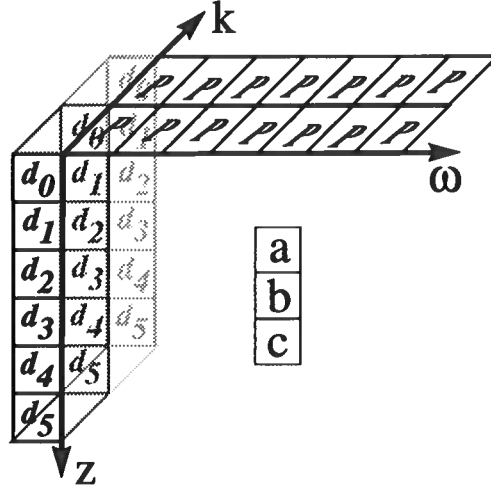
FIG. 4. The finite-difference mesh used in the modeling. The wavefield is computed by finite-differencing for each frequency and wavenumber.

(k).

$$\rho\frac{d}{dz}\frac{1}{\rho}\frac{d}{dz}P + \left(\frac{\omega^2}{v^2} - k^2\right)P = -\frac{\omega^2}{v^2}\delta(z - z_s)S(\omega), \tag{1}$$

where $\rho(z)$ is bulk density, z is depth, $v(z)$ is the medium velocity, $S(\omega)$ is the Fourier transformed signature of a source located at depth z_s, and $P(\omega, k, z)$ is the pressure field. Equation (1) may be solved by a second-order implicit finite-difference scheme. Figure 4 shows the finite-difference "star" used to calculate $P(\omega, k, z)$ for a single frequency and wavenumber. For each frequency and wavenumber, finite-differencing is performed for all depths with three coefficients: a, b and c, which vary with velocity and density, and a table d, which is associated with the source. This finite-difference scheme is described in Appendix A.

Using the finite-differencing derived in Appendix A, equation (1) is discretized into a set of tri-diagonal linear equations,

$$\begin{bmatrix} b_0 & c_0 & 0 & \cdots & 0 \\ a_1 & b_1 & c_1 & 0 & \vdots \\ 0 & a_2 & b_2 & c_2 & \vdots \\ \vdots & \ddots & \ddots & \ddots & \ddots \\ 0 & \cdots & \cdots & a_{n-1} & b_{n-1} \end{bmatrix} \begin{bmatrix} P_0 \\ P_1 \\ \vdots \\ P_{n-2} \\ P_{n-1} \end{bmatrix} = \begin{bmatrix} d_0 \\ d_1 \\ \vdots \\ d_{n-2} \\ d_{n-1} \end{bmatrix}. \tag{2}$$

The coefficients a_j, b_j, c_j, and the table d of this linear system are given by equations (A-9), (A-11), and (A-12). This tri-diagonal linear system can be solved using a linear recursion (e.g., Claerbout, 1985, p.99).

8

As shown in Appendix B, this second-order finite-difference scheme approximates the differential equation (1) to an fourth-order accuracy. The accuracy of this finite-difference algorithm is discussed in the section on Computational Issues (page 11).

Composing the Seismic Wavefield

The seismic wavefield is obtained by integrating the frequency-wavenumber response computed by the finite-differencing. For a line-source, or *a two-dimensional (2-D) point source*, the integration is a 2-D inverse Fourier transform of the frequency-wavenumber response,

$$p(t, r, z) = \frac{1}{4\pi^2} \int_{-\infty}^{\infty} d\omega e^{-i\omega t} \int_{-\infty}^{\infty} dk e^{ikr} P(\omega, k, z), \tag{3}$$

where r is the horizontal distance from the source, $k = k_x$ is the horizontal wavenumber, and $p(t, r, z)$ is the wavefield corresponding to a 2-D point source. For a three-dimensional (3-D) point source, a cylindrical coordinate system is used in the computation. The wavefield is circularly symmetric because of the layered-medium and the point pressure source. In this case, the solution is represented by

$$p(t, r, z) = \frac{1}{4\pi^2} \int_{-\infty}^{\infty} d\omega e^{-i\omega t} \int_{-\infty}^{\infty} dk k J_0(kr) P(\omega, k, z), \tag{4}$$

where r is the radial distance from the source, $k = \sqrt{k_x^2 + k_y^2}$ is the radial wavenumber, and $p(t, r, z)$ is the wavefield corresponding to a 3-D point source; k_x and k_y are wavenumbers related to two orthogonal horizontal directions in Cartesian coordinates.

The integral over the horizontal wavenumber in equation (3) is a straightforward inverse Fourier transform. However, the integral over the radial wavenumber in equation (4) is a Hankel transform, which has a non-periodic, Bessel function kernel. The computational costs of commonly used Hankel transform algorithms are of order $O(N^2)$ (Deng, 1991), where N is the number of samples to be transformed. The use of the fast Hankel transform algorithm can reduce the cost to an order of $O(NlogN)$, so that the efficiency of computing the seismic wavefield due to a 3-D point source is greatly enhanced (Deng, 1991). Further discussion of the seismic wavefield due to a 3-D point source, however, is beyond the scope of this thesis. Here, only those waves due to 2-D point sources are considered. Therefore, the wavenumber integral is simply performed by an FFT algorithm.

To satisfy the condition of causality, the integration over the frequencies in equation 3 is taken above the singularities on the real axis,

$$\omega = \nu + i\epsilon, \quad \text{where} \quad \epsilon > 0. \tag{5}$$

The frequency-wavenumber response $P(\omega, k, z)$ is thus computed for complex frequencies ω. As a result of using complex frequencies, the wavefield is exponentially attenuated by an amplitude factor $e^{-\epsilon t}$. This attenuation avoids the possible alias
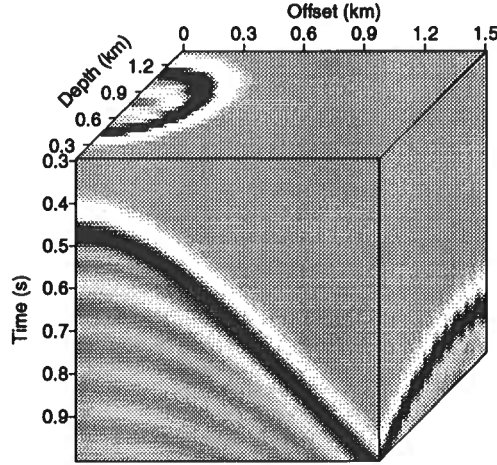
FIG. 5. Seismic wavefield in an increasing-trend, velocity-layered medium due to a 2-D point source buried at 0.75 km of depth. The velocity has a linear trend of $1.6 + 0.5z$ (km/s). The spatial wavelength of the velocity layering is 0.1km. The source wavelet is a Ricker wavelet with a dominant frequency of 8 Hz. For display purposes, the wavefield shown in the cube is sliced at 0.3 s in time and 0.3 km in depth.

of seismic traces, wherein signals of late times appear at early times on a seismogram. $P(\omega, k, z)$ is obtained by solving the complex-coefficient, tri-diagonal linear system, equation (2). Therefore, the wavefield corresponding to a 2-D point source is represented by

$$
\begin{aligned}
p(t, r, z) &= \frac{1}{4\pi^2} \int_{-\infty}^{\infty} d\omega e^{-i\omega t} \int_{-\infty}^{\infty} dk \, e^{ikr} P(\omega, k, z) \\
&= \frac{1}{4\pi^2} e^{\epsilon t} \int_{-\infty}^{\infty} d\nu e^{-i\nu t} \int_{-\infty}^{\infty} dk \, e^{ikr} P(\omega, k, z).
\end{aligned}
\tag{6}
$$

As shown in equation (6), the frequency integral is performed by a Fourier transform followed by an amplitude correction that compensates for the use of complex ω by an exponential factor $e^{\epsilon t}$ in the time domain. Hence, use of a large imaginary part of frequency can result in boosted noises at late times. An imaginary part $\epsilon = log_e(100)/T$, where T is the maximum recording time, keeps the amplitude factor to be at most 100 at the latest time. This choice of ϵ is used in this thesis research.

Figure 5 shows a seismic wavefield computed by using the FKFD modeling algorithm for an increasing-trend, velocity-layered medium. This type of medium is used for the study of dip-dependent attenuation of seismic waves described on page 17.

Green's Function

The Green function is the wavefield that corresponds to an impulse source function both in time and space, $s(t, x, z) = \delta(t)\delta(x - x_s)\delta(z - z_s)$. If the Green function for a single frequency is $G(\omega, x, z; x_s, z_s)$, then according to the representation theorem (e.g., Aki et al., 1980, p.28), the wavefield for a single frequency $P(\omega, \xi, \eta)$ due to a source function $\tilde{S}(\omega, x, z)$ can be written as,

$$P(\omega, x, z) = \int_{-\infty}^{\infty} d\xi \int_{-\infty}^{\infty} d\eta \tilde{S}(\omega, \xi, \eta) \, G(\omega, x, z; \xi, \eta). \tag{7}$$

Therefore, computing the Green function can be an important step for obtaining the seismic wavefield. Solving equation (1) via the finite-differencing with $S(\omega) = 1$ yields a frequency-wavenumber response of the Green function.

Computational Issues

The ability to handle rapid vertical variation in velocity functions is an advantage of finite-difference algorithms over some other approaches for computing seismic wavefields, such as ray tracing or reflectivity. Since the computational cost of solving the tri-diagonal linear system, equation (2), is determined by the size of the system, the cost of the FKFD modeling is directly related to the number of vertical samples, as opposed to the cost of reflectivity methods, which depends on the number of layers.

However, finite-difference methods have the disadvantage of introducing errors as a result of approximating differential operators. The accuracy of a finite-difference algorithm is an important issue in the computation; therefore, grid spacings must be carefully chosen to ensure both accuracy and efficiency.

To determine the grid spacing in finite-differencing, two issues need to be considered: the wavelength of the seismic signal, and the thickness of layers. According to the sampling theorem, signals must be sampled at least twice in each cycle, or

$$\Delta z \le \frac{v}{2f_{max}} = \frac{\pi v}{\omega_{max}},$$

where f_{max} is the maximum frequency of the signal and $\omega_{max} = 2\pi f_{max}$. However, approximations to differential operators require a smaller grid spacing than that required by the sampling theorem. Define a dimensionless *grid spacing parameter R* for measuring the grid spacing with respect to a seismic signal,

$$R \equiv \frac{\omega_{max}\Delta z}{\pi v_{min}},$$

where v_{min} is the minimum velocity of the medium. From this definition, R is the ratio of the grid spacing used in approximating differential operators to the maximum spacing required by the sampling theorem. In addition, the medium must be sampled at least once for each layer. Therefore, the grid spacing used in the finite-differencing is determined by

$$\Delta z = MIN\left(\frac{\pi v_{min}}{\omega_{max}}R, h_{min}\right), \tag{8}$$

11

where h_{min} is the minimum thickness of the layers. Hence, the cost of a finite-difference algorithm depends on both the wavelength of seismic waves and the minimum thickness of layers.

The grid dispersion and anisotropy of the numerical approximation can be represented by the deviation of the phase velocity of waves in the numerical solution c from the real velocity of the medium v. According to discussions in Appendix B, the phase velocity of waves numerically propagating on the grid is a function of the propagation angle and frequency,

$$c(\theta, \omega) \approx \frac{v}{\sqrt{1 - \left(\frac{\pi v_{min}}{v \omega_{max}}\right)^4 \frac{\omega^4 R^4 \cos^6 \theta}{240}}}. \tag{9}$$

Figure 6 shows the ratio of the phase to true velocity as a function of frequency and propagation angle at the minimum velocity. Because the phase-velocity error decreases as frequency decreases or propagation angle increases, horizontal traveling waves have the least phase-velocity error caused by finite-differencing. The phase-velocity error at the maximum frequency is determined by the grid spacing parameter R. Figure 7 shows the phase-velocity error at the maximum frequency and the minimum velocity for $R = 0.2$ and $R = 0.4$. It can be seen that halving R greatly improves the accuracy of the approximation. All the numerical results in this thesis are generated by the finite-difference algorithm with $R = 0.4$ because the finite-difference approximation is accurate enough for the requirement of this research.

Brown (1984) showed that a centered finite-difference approach for piecewise smooth coefficients converges to a true solution of the problem in the limit of the grid spacing going to zero. According to the previous discussions, the convergence rate of the phase velocity is of fourth-order in grid spacing. However, the order of convergence of amplitudes is another issue that must be considered. According to Brown (1984), the accuracy of the phase-velocity is determined by the approximation to differential operators within layers, and the accuracy of reflection amplitude is determined by the interface approximation – the continuity of the wavefield at interfaces of layers and the continuity of the gradient of the wavefield at the normal direction of these interfaces. According to Sochacki, et al. (1991), the centered difference scheme described in Appendix A implies a second order, $O(\Delta z^2)$, approximation of this interface condition.
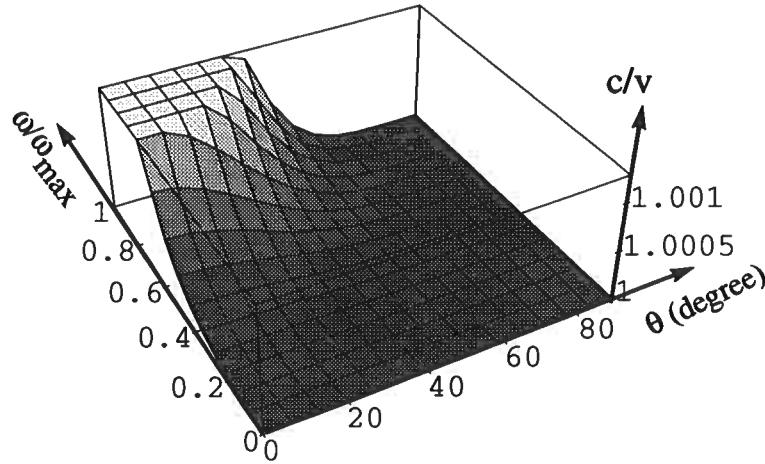
12

FIG. 6. The accuracy of the finite-difference scheme used in the modeling. The ratio of the numerical and material velocity as a function of frequency and propagation angle. The grid parameter R is 0.4. For a fixed grid parameter R, the dispersion and anisotropy of the finite-difference decreases with decreasing frequency and with increasing propagation angle.

Zero-Offset Reflections from Dipping Interfaces in Thinly-Layered Media

Born Approximation

The reflected wavefield is often referred to as the *scattered wavefield*, while the wavefield corresponding to the Green function is the *incident wavefield* (e.g., Bleistein, 1984). Under the assumption of small reflection coefficients, a first-order Born approximation (e.g., Bleistein, 1985) gives zero-offset reflections from a dipping interface using the incident wavefield.

For our problem, the velocity of the sedimentary medium is taken as the *background velocity*, and the presence of an interface perturbs the velocity function. As a result of this perturbation, the real velocity of the model, which is made up of a sequence of sedimentary layers and an interface, may vary laterally as well as vertically. If the background velocity function is $c(z)$ and the real velocity function of the model is $v(x, z)$, the perturbation $\alpha(x, z)$ due to the interface is defined by the expression

$$\frac{1}{v^2(x, z)} = \frac{1}{c^2(z)} \left[1 + \alpha(x, z)\right]. \tag{10}$$
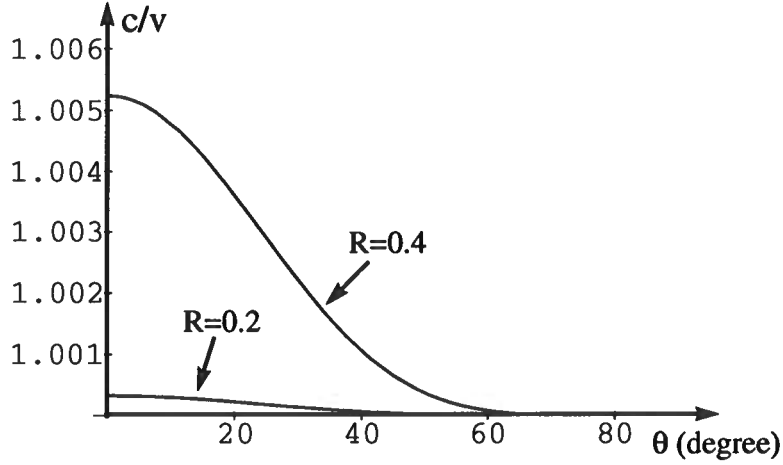
13

FIG. 7. Phase-velocity accuracy of the finite-difference algorithm at the maximum frequency. The ratio of the numerical and real velocity as a function of the propagation angle for two grid parameters, $R = 0.2$ and $R = 0.4$. The halving of R greatly improves the accuracy of the approximation.

The wavefield for a single frequency, $P(\omega, x, z)$, is the solution of the 2-D Helmholtz equation

$$\rho \frac{\partial}{\partial z} \left(\frac{1}{\rho} \frac{\partial}{\partial z} P \right) + \frac{\partial^2}{\partial x^2} P + \frac{\omega^2}{v^2(x, z)} P = -\frac{\omega^2}{v^2(x_s, z_s)} \delta(x - x_s) \delta(z - z_s) S(\omega), \quad (11)$$

where $S(\omega)$ is the Fourier transformed signature of a source located at (x_s, z_s). This wavefield is made up of two parts, the incident and scattering fields:

$$P(\omega, x, z) = P_i(\omega, x, z) + P_s(\omega, x, z). \quad (12)$$

The incident field $P_i(\omega, x, z)$ is a solution of the *unperturbed* Helmholtz equation,

$$\rho \frac{\partial}{\partial z} \left(\frac{1}{\rho} \frac{\partial}{\partial z} P_i \right) + \frac{\partial^2}{\partial x^2} P_i + \frac{\omega^2}{c^2(z)} P_i = -\frac{\omega^2}{v^2(x_s, z_s)} \delta(x - x_s) \delta(z - z_s) S(\omega). \quad (13)$$

If $G(\omega, x, z; x_s, z_s)$ is the Green function for a single frequency due to a 2-D point source at (x_s, z_s), then we have

$$P_i(\omega, x, z) = S(\omega) \, G(\omega, x, z; x_s, z_s). \quad (14)$$

As the horizontal dependence of the wavefield depends only on the distance from the source, equation (14) can be equivalently written as,

$$P_i(\omega, |x - x_s|, |z - z_s|) = S(\omega) \, G(\omega, |x - x_s|, |z - z_s|). \quad (15)$$

14

The Green function $G(\omega, |x - x_s|, |z - z_s|)$ can be obtained by the FKFD algorithm mentioned in the previous section.

The equation for the scattered field given below is obtained by substituting equations (10) and (12) into the Helmholtz equation (11),

$$\rho\frac{\partial}{\partial z}\left(\frac{1}{\rho}\frac{\partial}{\partial z}P_s\right) + \frac{\partial^2}{\partial x^2}P_s + \frac{\omega^2}{c^2(z)}P_s = -\frac{\omega^2}{c^2(z)}\alpha(x, z)\left[P_i + P_s\right]. \tag{16}$$

In equation (16), P_s is $O(\alpha)$, linear order in α (Bleistein, 1985); the second-order term αP_s at the right-hand side of equation (16) can be ignored if α is small enough that $O(\alpha^2)$ is negligible. Therefore, the scattering field P_s is a solution of the Helmholtz equation where the velocity function is the background velocity $c(z)$ and the source function is a scaled incident field αP_i. Referring to equation (7), the solution of equation (16) at (x, z) is

$$P_s(\omega, x, z) = \omega^2 \int_{-\infty}^{\infty} d\xi \int_{-\infty}^{\infty} d\eta \frac{\alpha(\xi, \eta)}{c^2(\eta)} P_i(\omega, |\xi - x_s|, |\eta - z_s|) G(\omega, |x - \xi|, |z - \eta|). \tag{17}$$

If the source and receiver locations are the same, as for a zero-offset seismic experiment, then

$$P_s(\omega, x_s, z_s) = \omega^2 S(\omega) \int_0^{\infty} d\eta \frac{1}{c^2(\eta)} \int_{-\infty}^{\infty} d\xi \alpha(\xi, \eta) G^2(\omega, |\xi - x_s|, |\eta - z_s|). \tag{18}$$

Equation (18) is obtained from equation (17) by the fact that $\alpha(x, z) = 0$ for $z < 0$, changing the order of integration and substituting in equation (15). Equation (18) represents a zero-offset section reflected from an interface that perturbs the background velocity $c(z)$ with a perturbation $\alpha(x, z)$.

Line Integral in Born Approximation

The perturbation function α, due to a 2-D geologic structure, is non-zero in the area covered by the structure. Hence strictly, the computation of zero-offset seismograms using equation (18) requires an areal integration. However, in this research, I have assumed that the perturbation exists only on the interface,

$$\alpha(x, z) = \tilde{\alpha}(x, z)\delta(x - x_r)\delta(z - z_r),$$

where (x_r, z_r) lies on the interface. Under this assumption, the double integral in equation (18) is reduced to a line integral along the interface L,

$$P_s(\omega, x_s, z_s) = \omega^2 S(\omega) \int_L dl(\xi, \eta) \frac{1}{c^2(\eta)} \tilde{\alpha}(\xi, \eta) G^2(\omega, |\xi - x_s|, |\eta - z_s|), \tag{19}$$

where $l(\xi, \eta)$ is the arc length of the interface at (ξ, η). This delta-function perturbation assumption reduces the computation from the area integral to a line integral. However, the use of a delta function introduces a spatial differentiation to wavelets

because of the reduction from an areal integration to a line integration. Since the purpose of this research is to study the behavior of seismic waves caused by velocity layering, and as the same differentiation will occur with or without the layering, this differentiation of wavelets does not affect the result of this research.

According to Bleistein (1985), the first order Born approximation described above is valid for perturbations $\alpha < 5\%$. Throughout this thesis, $\alpha = 2.5\%$ is used in all the experiments for analyzing the dip-dependent behavior of the seismic waves in thinly-layered media.

Theoretically, using equation (19) with a layered background medium can yield zero-offset reflections from an arbitrarily shaped interface. However, the algorithm required to numerically represent an arbitrary geometry is not trivial. Fortunately, for the purpose of studying the dip-dependent behavior of seismic waves, only plane-dipping interfaces are necessary. The dip-dependent behavior of waves traveling in velocity layered media is to be studied by observing seismograms generated by this modeling algorithm.

FREQUENCY-DEPENDENT ATTENUATION OF SEISMIC WAVES

Attenuation of Seismic Waves in Thinly-Layered Media

Amplitudes of seismic waves are altered in a frequency-dependent way while they propagate. It is well known that seismic waves lose their high frequencies because some of the high-frequency energy is absorbed by the medium due to inelasticity. Therefore, seismic data lose temporal resolution at late recording times. This frequency-dependent attenuation is quantitatively described by the "Q" of the medium. The change in the frequency content of seismic data with increase of recording time is a form of *non-stationarity*.

Seismic deconvolution is designed to improve the temporal resolution of seismic data. When the non-stationarity of seismic waves cannot be ignored, the deconvolution process must treat seismic data recorded at late times differently from those recorded at earlier times. *Time-variant spectral whitening* (e.g., Yilmaz, 1987, 147) is a straightforward technique of deconvolution for compensating for the non-stationarity and thus enhancing the temporal resolution of seismic data. *Inverse Q-filtering* deconvolution (e.g., Yilmaz, 1987, 151) is a more appropriate technique than time-variant spectral whitening for dealing with the frequency-dependent attenuation because this deconvolution approach is based on an understanding of the physical mechanism that causes the phenomenon.

Observations of seismic data indicate that attenuation of seismic waves can be caused by other mechanisms. Figure 8 shows reflections from a horizontal interface beneath two different sedimentary media, one with a linear velocity variation without layering, and the other with an increasing-trend, velocity-layered medium. These reflections are computed by the modeling method described in the section on Modeling of Seismic Waves in Thinly-Layered Media (page 7). Figure 8a shows the reflection for the linear-velocity medium. The layered medium, corresponding to Figure 8b, has a spatial wavelength smaller than the dominant wavelength of the seismic signal. The reflection wavelet for the layered medium is broader than that for the medium without layering. Broadening of the wavelet shows that some of the high-frequency energy is lost through reflection as waves travel in the thinly-layered medium. This phenomenon can be seen clearly in Figure 9, which shows the frequency spectra of these two reflections. Because both of the media have large Q, the absorption of seismic energy due to inelasticity can be ignored. The loss of high-frequency content in Figure 8b can be attributed only to the thin layering of the medium.

O'Doherty and Anstey (1971) observed that the high-frequency content of seismic waves appears to be attenuated by short-period multiples. When seismic waves travel through a sequence of sedimentary layers, a series of multiples is produced at velocity discontinuities. These multiples cannot be distinguished individually if thicknesses of the layers are smaller than the seismic wavelength. Seismic wavelets, which are the superpositions of both primaries and multiples, are thereby broadened in time. As a result of these interferences, seismic waves lose their high frequencies as they
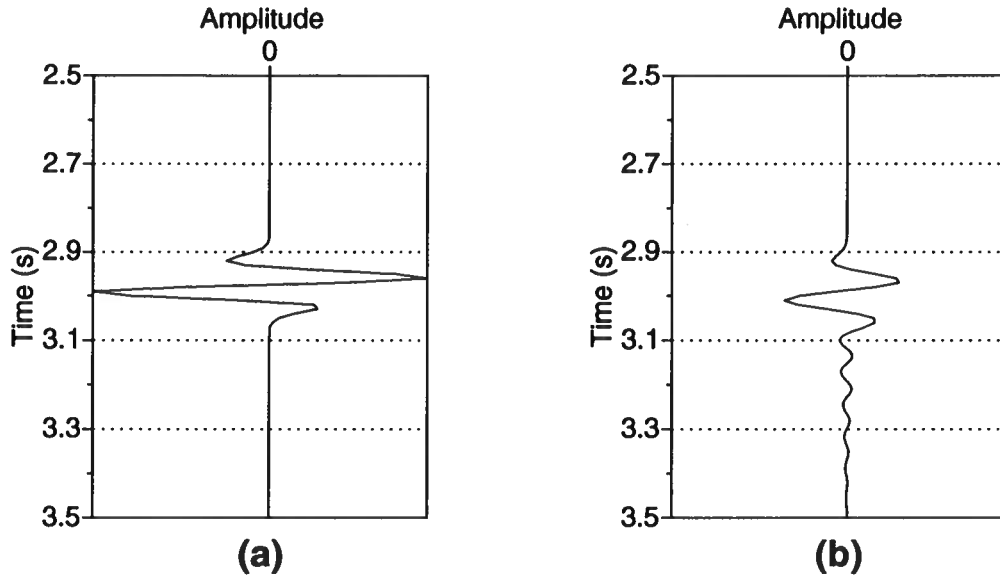
FIG. 8. Zero-offset reflections from a horizontal interface beneath (a) a linear-velocity medium $(v(z) = 1.6 + 0.5z$ (km/s)) and (b) an increasing-trend, velocity-layered medium where the velocity has a linear trend of $1.6 + 0.5z$ (km/s) plus a sinusoidal variation with a spatial wavelength 60 m. The dominant frequency of the source signal is 10 Hz.

travel through a sequence of thin layers. This phenomenon is known as *stratigraphic filtering*. Though this effect on seismic signals is similar to that caused by inelasticity, the stratigraphic filtering effect is due to destructive interference, not to absorption of seismic energy.

Following O'Doherty and Anstey (1971), much progress has been made toward understanding the attenuation behavior of seismic waves due to thin layers. Banik et al. (1985a) derived formulas to describe quantitatively the apparent attenuation and time delay caused by stratigraphic filtering in a statistical sense. In addition, they studied this filtering for sedimentary sequences typically logged in oil and gas wells (Banik et al., 1985b).

However, their work was based on an assumption that seismic waves propagate *vertically* through sedimentary layers (i.e., perpendicular to the reflecting boundaries). Seismic waves reflected from a steep interface have to spend a significant amount of time traveling more or less horizontally. These waves, traveling at large incident angles may be attenuated and dispersed by another, not well-known reason. Successful imaging of steep geologic subsurfaces likely requires that the behavior of horizontally traveling waves be understood.
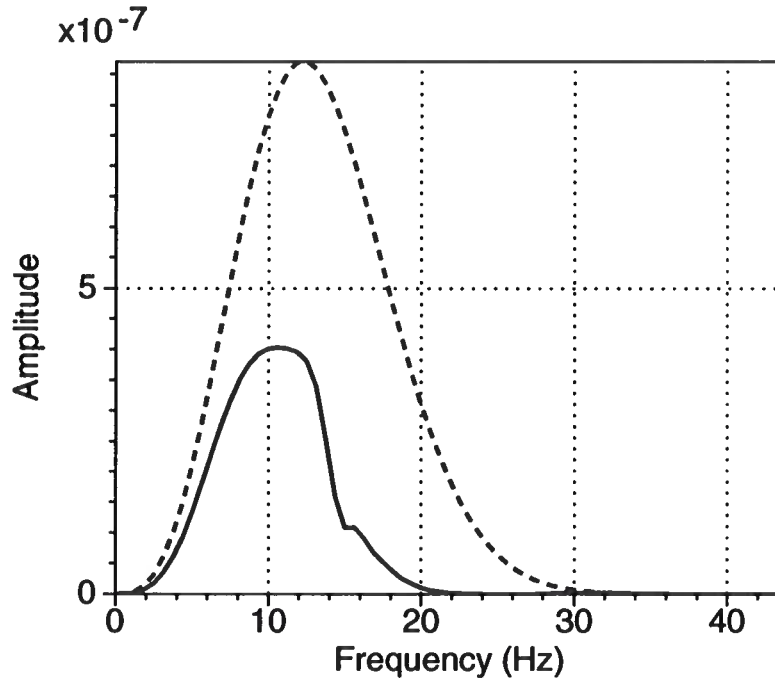
18

FIG. 9. Frequency spectra of the seismic traces in Figure 8. The dotted line is the frequency spectrum of the reflection for the linear-velocity medium without layering, as in Figure 8a. The solid line is the spectrum of the reflection for the increasing-trend, velocity-layered medium, as in Figure 8b.

Figure 10 shows reflections from a *vertical* interface in two different sedimentary media, a linear-velocity medium without layering (Figure 10a) and an increasing-trend, velocity-layered medium (Figure 10b) with a spatial wavelength comparable to the dominant wavelength of the seismic signal. As was the case for vertical incidence, the reflection wavelet for the layered-medium arrives at the same time as that for the linear velocity medium, but is broader. In addition, the wavelet for the layered medium has lower amplitude than that for the linear-velocity medium. The frequency spectra shown in Figure 11 highlight differences in these two reflections. High frequencies in the waves that travel nearly horizontally in the layered medium are largely attenuated – more so than are those in vertically propagating waves.

As observed in Figure 8 and Figure 10, seismic waves reflected from horizontal and vertical interfaces are attenuated and dispersed differently. It is known that the attenuation of waves reflected from horizontal interfaces arises from stratigraphic filtering associated with short-period multiples. However, because of ray bending, those waves reflected from vertical interfaces spend more time traveling in each layer and travel through fewer layers than do those reflected from horizontal interfaces. Therefore,
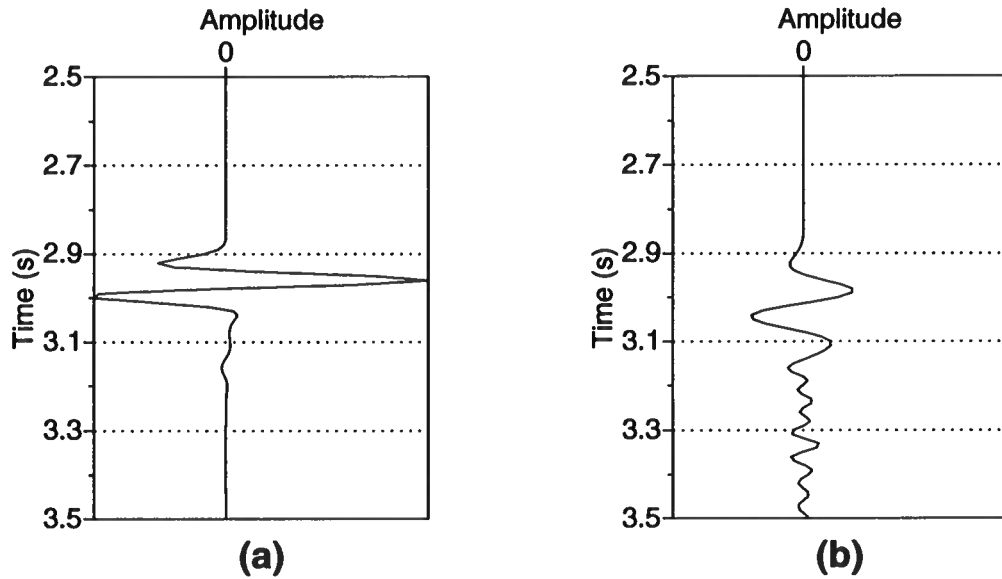
FIG. 10. Zero-offset reflections from a vertical interface. (a) is the reflection for a linear-velocity medium. The velocity function is $v(z) = 1.6 + 0.5z$ (km/s). (b) is the reflection for an increasing-trend layered-velocity medium. The velocity function has a linear trend of $1.6+0.5z$ (km/s) plus a sinusoidal variation with a spatial wavelength 150 m. The dominant frequency of the source signal is 10 Hz. The horizontal distance from the source to the vertical interface is 2.5 km.

the stratigraphic filtering of waves reflected from steep interfaces will be different, and perhaps less severe. However, from our previous observations in Figure 3, waves reflected from a vertical interface are more dispersed than are those reflected from a horizontal interface. This implies that there must be another mechanism that contributes to the attenuation of seismic waves that propagate with large, non-vertical angles.
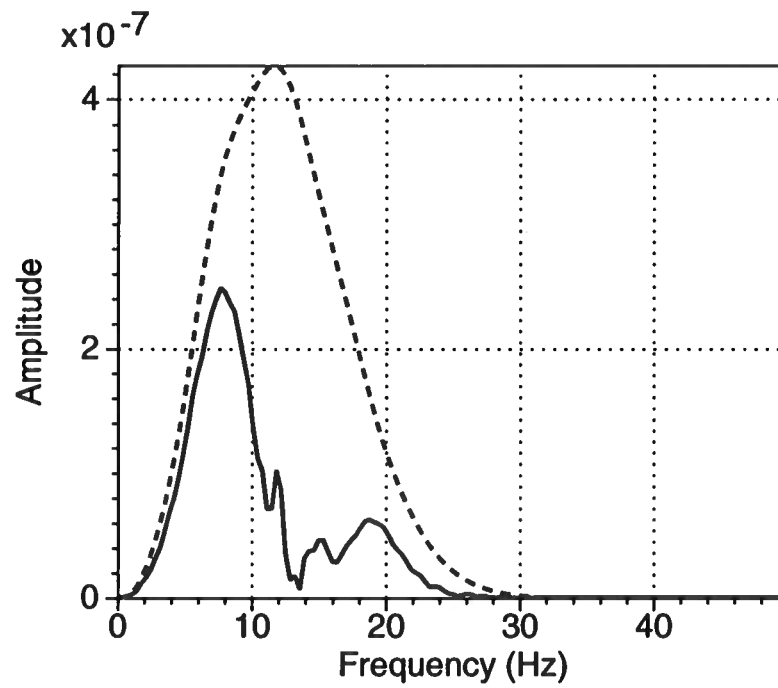
FIG. 11. Frequency spectra of the seismic traces in Figure 10. Dotted line is the frequency spectrum of the reflection for the linear-velocity medium without layering, as in Figure 10a. Solid line is the spectrum of the reflection for the increasing-trend, velocity-layered medium, as in Figure 10b.

Tunneling across a Thin High-Velocity Layer

According to Snell's law, the transmission angle for seismic waves transmitted from a low- to a high-velocity medium is larger than the incident angle. The critical angle is the incident angle which produces a 90° transmission angle at the interface of a velocity discontinuity. When seismic waves reach a high-velocity medium with angles equal to or larger than the critical angle, no waves propagate into the high-velocity medium. However, some of the seismic energy, which has an exponentially decaying amplitude with distance from the boundary, penetrates through the discontinuity into the high-velocity medium. This penetrating energy is known as an *evanescent wave* (e.g., Aki et al., 1980, 155). The decay rate of the evanescent wave is a function of frequency,

$$A \propto \exp\left(-\omega z \sqrt{\frac{\sin^2 \theta_1}{v_1^2} - \frac{1}{v_2^2}}\right), \tag{20}$$

where ω is the frequency of the wave, θ_1 is the incident angle of the wave, v_1 is the velocity of the low-velocity medium, and v_2 is the velocity of the high-velocity medium. The rate of amplitude decay increases linearly with frequency, and the decay rate also depends on the incident angle and the velocity contrast between the two media. Figure 12 shows snapshots of seismic waves from a point source propagating before and after reaching the critical angle. After the waves reach the *critical distance*, which is the offset at which the reflection occurs at the critical angle, the amplitudes of reflections are stronger than those of smaller offset reflections while the transmitted waves become evanescent.

If the high-velocity layer is thin relative to the wavelength of seismic waves, the evanescent waves may reach the boundary of another low-velocity layer and become propagating again. Figure 13 illustrates the point made in equation (20) that high-frequency evanescent energy decays faster than does low-frequency energy. Therefore, more low-frequency evanescent energy arrives at the lower boundary of the high-velocity layer than does high-frequency energy. Propagating waves in the deeper low-velocity layer are dominated by the low frequencies, since their high-frequency content cannot be recovered. This low-frequency leakage when seismic waves travel through a thin, high-velocity layer is known as *tunneling*. Figure 13 also shows that the waves arriving at the critical angle are better able to tunnel through the thin, high-velocity layer than are waves arriving at larger angles.

Figure 14 shows seismic waves propagating in a three-layer medium that has a high-velocity layer between two low-velocity layers. When the wave reaches the first interface with a post-critical angle, the energy penetrating into the high-velocity layer becomes evanescent. If the thickness of the high-velocity layer is large relative to the seismic wavelength, amplitudes of the reflections are strong after the waves reach the critical angle and transmitted waves become evanescent, as shown in Figure 14a. Hardly any evanescent energy survives the 300 m thick high-velocity layer at offsets
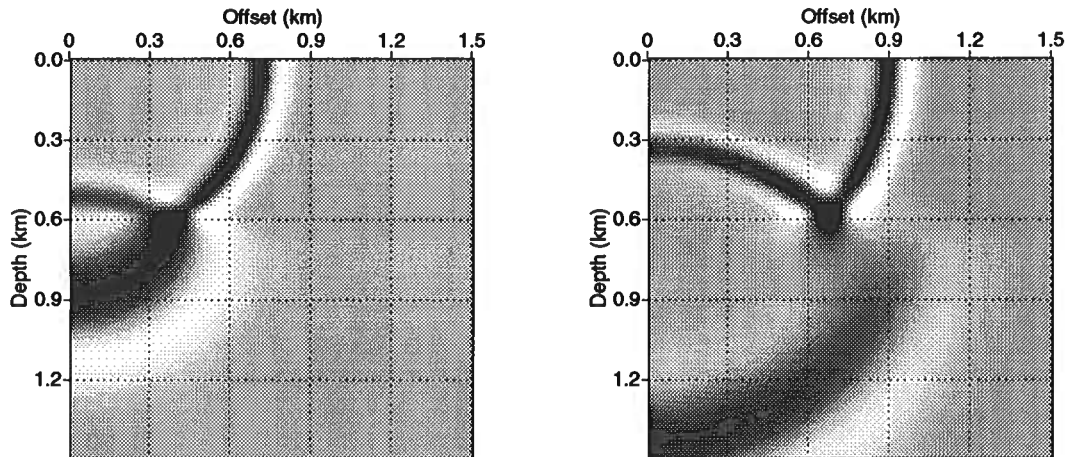
FIG. 12. Snapshots of seismic wave propagation, computed for a 2-D point source at the origin. The waves propagate through a velocity discontinuity of the medium at $z = 0.6$ km, where $v_1 = 2$ km/s, $v_2 = 6$ km/s. The critical distance is 0.42 km. The dominant frequency of the source signal is 10 Hz. (left): the snapshot before the waves reach the critical angle. (right): the snapshot after the waves reach the critical angle. Notice the stronger amplitude of reflections that beyond critical distance than those of smaller offset reflections, and the exponentially decaying evanescent energy just below a depth of 0.6km of waves.

larger than the critical distance. Figure 14b contains a snapshot of propagating waves at a later time; the increased incident angle at the interface increases the decaying rate of evanescent waves and even less energy is observed in the deeper low-velocity layer than at the earlier time. Figure 14c shows the snapshot for a 75 m thick high-velocity layer; the reflections at offsets larger than the critical distance are not as strong as those shown in Figure 14a. Some of the evanescent frequencies in the thin, high-velocity layer reach the lower low-velocity medium before their amplitudes decay to negligible values. Figure 14d shows that less energy tunnels through the thin, high-velocity medium at larger offsets, but much more has tunneled through this thinner layer than through the thicker ones.

Observations of seismic waves propagating in this three-layer medium tell us that evanescent energy can tunnel through high-velocity layers if the high-velocity layer is *thin* enough for the propagating energy to survive. The amount of energy that survives is determined by the frequency content of the seismic signal, the propagation angle, the velocity contrast of the low- and high-velocity media, and the thickness of the high-velocity layer.

The numerical results in Figure 12 and Figure 14 were produced by the frequency-wavenumber, finite-difference modeling method mentioned in the preceding chapter. This modeling method handles waves that tunnel through thin, high-velocity media,
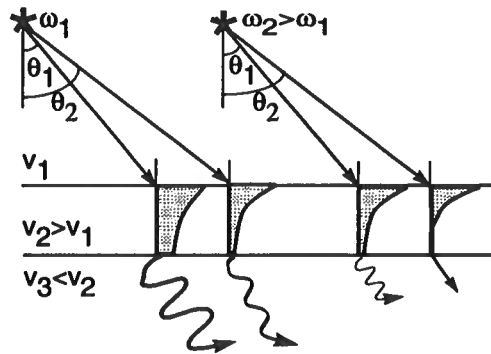
23

FIG. 13. Amplitudes of evanescent waves decay exponentially with depth. The decay rate is a function of the frequency and the incident angle. When the high-velocity layer is thin, some of the evanescent energy survives to propagate into the deeper medium. The low-frequency energy has more chance to tunnel through than does the high-frequency energy.

while conventional WKBJ methods cannot predict the low-frequency leakage of the evanescent waves.

When seismic waves are reflected from a steep interface in a medium with a sequence of sedimentary layers, low-frequency waves tunnel repeatedly through thin, high-velocity layers in the alternating sequence of high- and low-velocity layers. Waves traveling through the medium are those surviving this repeated tunneling, which introduces a frequency-dependent *evanescent filtering*. Therefore, seismic waves reflected from steep interfaces in thinly-layered media are attenuated and dispersed because of both their large propagation angles and the velocity layering.
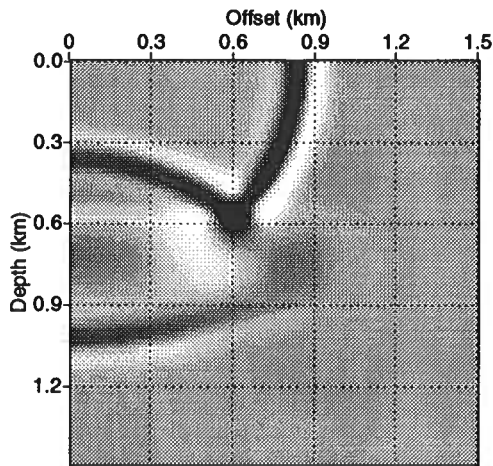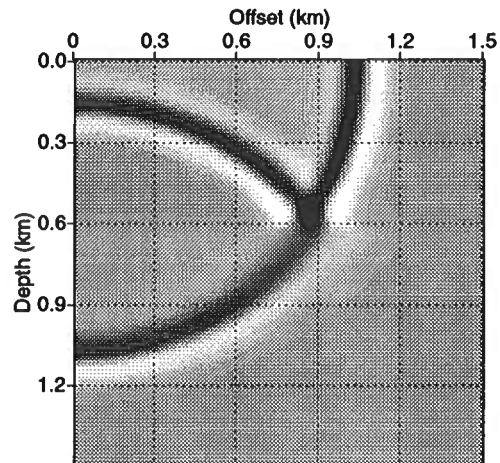
(a) layer=300 m time=0.52 s
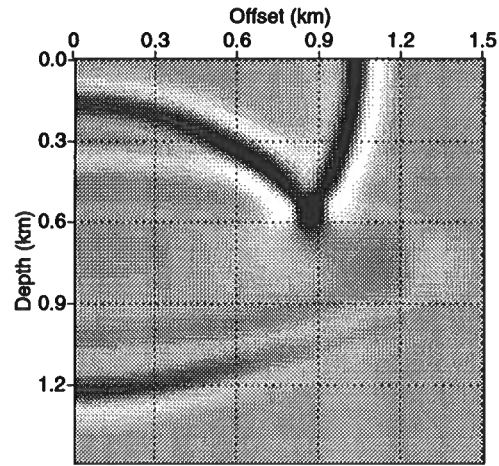
(b) layer=300 m time=0.62 s
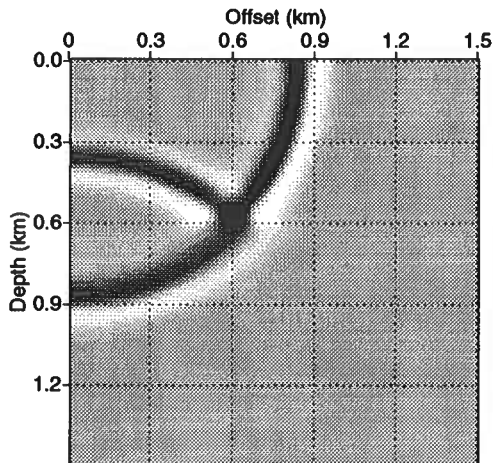
(c) layer=75 m time=0.52 s

(d) layer=75 m time=0.62 s

FIG. 14. Snapshots of seismic waves propagating through three-layer media with a $v_1 = 2\,\text{km/s}$ upper low-velocity layer, a $v_2 = 6\,\text{km/s}$ middle high-velocity layer, and a $v_3 = 2\,\text{km/s}$ lower low-velocity layer. The critical distance is 0.42 km. The dominant frequency of the source signal is 10 Hz. (a),(b): Snapshots of waves propagating at time $= 0.52\,\text{s}, 0.62\,\text{s}$ in a medium with a high-velocity layer between $z = 0.6$ and $0.9\,\text{km}$. (c),(d): Snapshots of waves propagating at time $= 0.52\,\text{s}, 0.62\,\text{s}$ in a medium with a high-velocity layer between $z = 0.6$ and $0.675\,\text{km}$.

Dip-Dependent Behavior of Seismic Waves in Thinly-Layered Media

Reflections from Vertical Interfaces

Due to evanescent filtering, seismic waves reflected from a vertical interface embedded in an increasing-trend, layered-velocity medium are attenuated and dispersed. The amount of energy loss due to evanescent filtering is determined by the spatial wavelength of the medium and the velocity contrast of low- and high-velocity layers. Keeping the velocity contrast of the sedimentary layers as a constant, changes in the spatial wavelength of the sedimentary layers greatly affects the evanescent filtering of seismic waves.

Figure 15 shows reflections from a vertical interface in an increasing-trend, velocity-layered medium where variation of the medium is slower than that of the waves. The increasing trend of velocity with depth causes ray bending of seismic waves. When these waves reach a high-velocity layer at post-critical angles, they become evanescent with exponentially decaying amplitudes. Waves reflected from a vertical interface in a thickly-layered medium, as shown in Figure 15a, have lost most of their energy due to alternation of the layers and large, non-vertical propagation angles of the waves. For comparison, Figure 15b shows the same reflections for linear-velocity medium without layering. The smoothness of the velocity function yields a high-resolution seismogram where no intra-bed multiples or evanescent waves are generated. However, when seismic waves are reflected from a vertical interface in an increasing-trend, velocity-layered medium, most of the energy is lost in the thick high-velocity layers.

Figure 16 shows the frequency-dependent behavior of waves reflected from a vertical interface in layered media with different layer thicknesses. The waves increase their propagation angles as they travel down to the interface due to the increasing-trend of velocity with depth; they normally reach the vertical interface and reflect back to the source position along the same paths. When the sedimentary layers are thick relative to the wavelength of seismic waves, repeated evanescent decay greatly attenuates the high-frequency energy. The low resolution and weak amplitudes of the waves in Figure 16a shows that only very low frequencies survive the evanescent filtering in the medium where velocity varies slowly with respect to the seismic wavelength. When the spatial wavelength of the sedimentary medium decreases, more and more energy tunnels through the thin, high-velocity layers. Figure 16 illustrates that resolution of the seismograms increases with a decrease in layer thickness. Figure 16d has the sharpest reflections of all four seismograms. When the spatial wavelength of the layered medium is shorter than the minimum wavelength of the seismic signal, most of the seismic energy survives the repeated thin high- and low-velocity alternating layers.

Figure 17 shows frequency spectra of the reflections in Figure 16. The spectra verify the observations from Figure 16 that frequency-dependent attenuation is more severe for larger ratio of changes of the medium to that of the wavefield. When layer thicknesses are comparable to the seismic wavelength, only low frequencies can
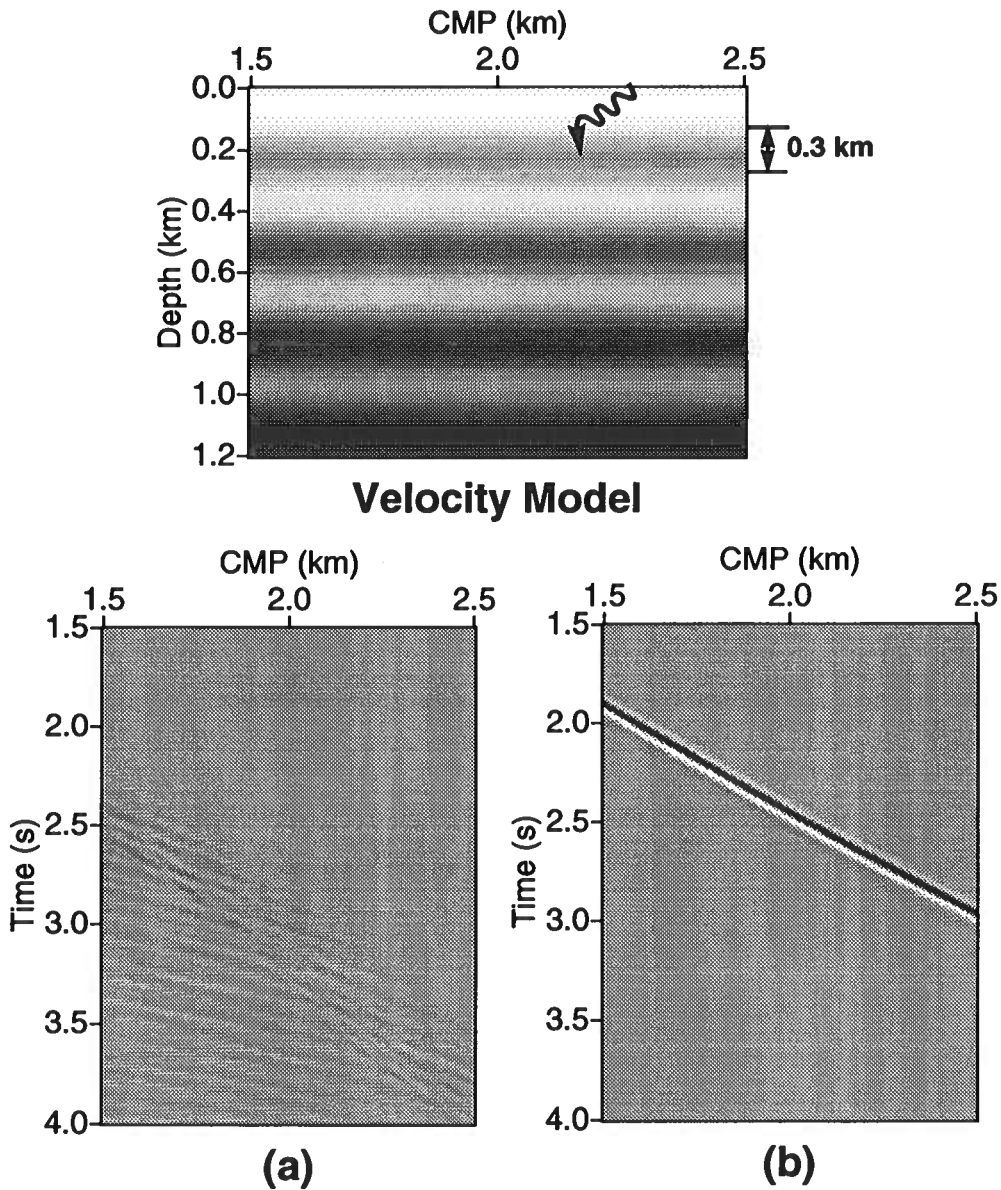
FIG. 15. Zero-offset synthetic reflections from a vertical interface. The seismogram in (b) is for a linear-velocity medium with a velocity function $v(z) = 1.6 + 0.5z$ (km/s). The upper figure shows the velocity model for the seismogram in (a). It is an increasing-trend, velocity-layered medium, which has a velocity trend of $1.6 + 0.5z$ (km/s); the spatial wavelength of the medium is 300 m. The dominant frequency of source wavelet is 10 Hz.
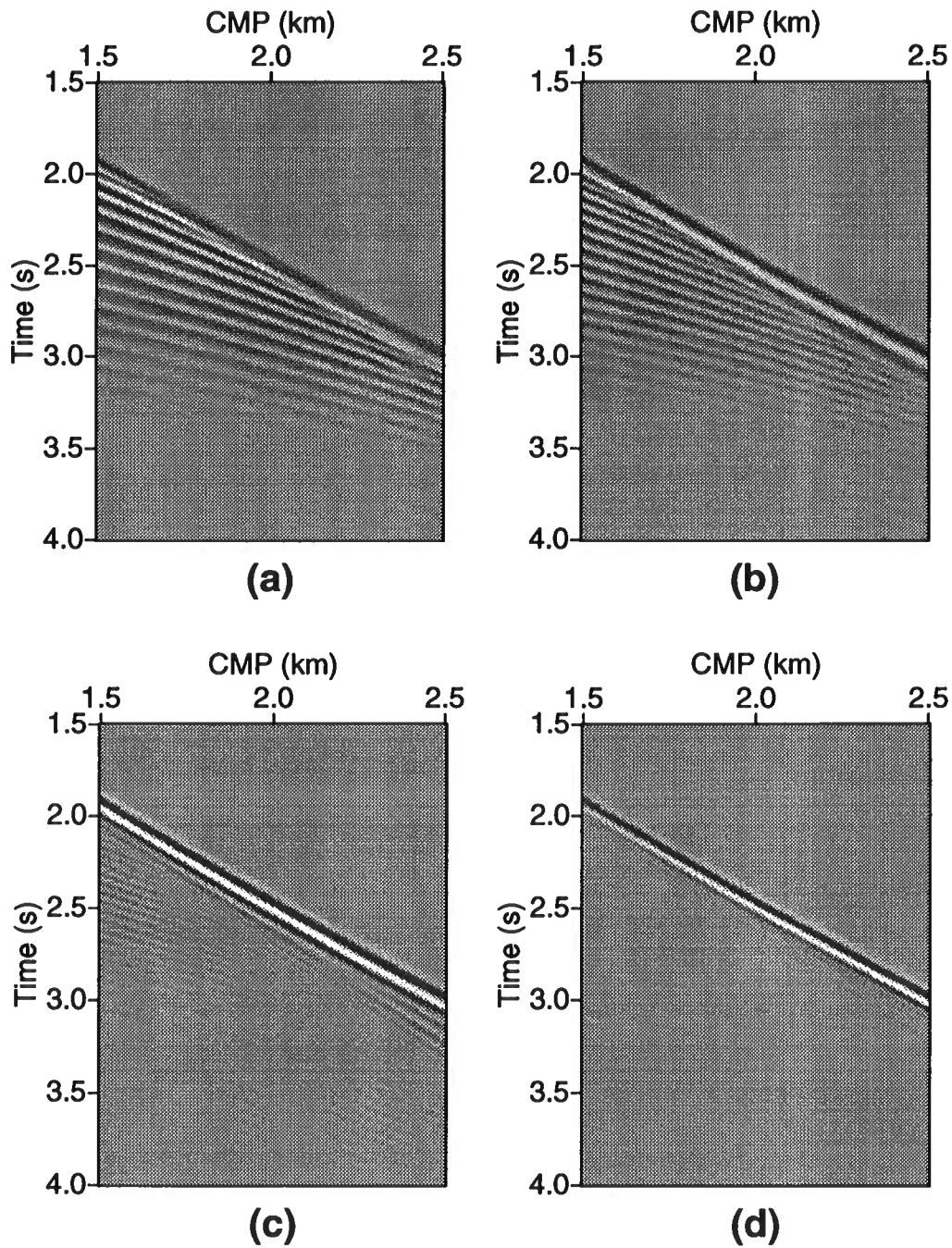
FIG. 16. Zero-offset reflections from a vertical interface in four layered media. The velocity in each medium has a linear trend of $1.6 + 0.5z$ (km/s) and a sinusoidal variation with spatial wavelength (a) 250 m, (b) 150 m, (c) 100 m and (d) 60 m, respectively. The dominant frequency of the source signal is 10 Hz.

survive the evanescent filtering. As layers of sedimentary media become thinner, progressively more high-frequency energy survives the thin, high-velocity layers. If the spatial wavelength of the medium is smaller than the minimum wavelength of the seismic signal, the shape of the frequency spectrum is similar to that for a medium without velocity-layering; seismic waves tunnel through the thin, high-velocity layers for all frequencies.
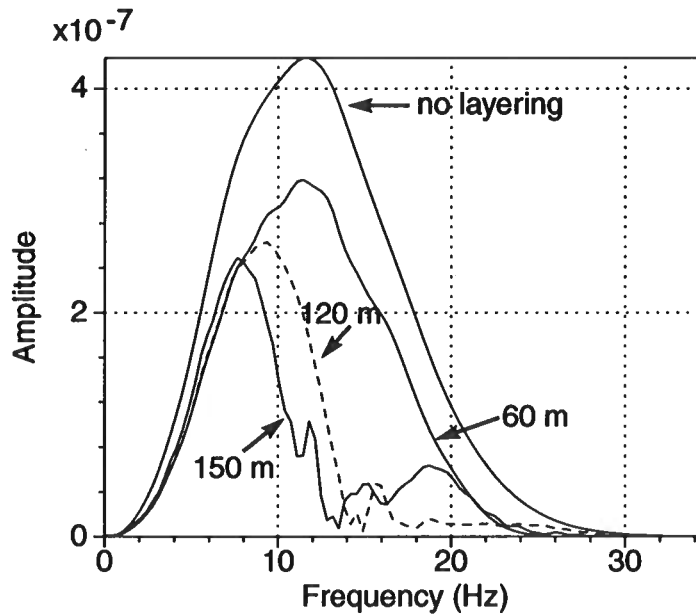
FIG. 17. Frequency spectra of the reflections from a vertical interface in four different layered media. The dominant frequency of the source signal is 10 Hz. The velocity in each of the media has a linearly increasing trend of $1.6 + 0.5z$ (km/s). One medium has no velocity-layering. The spatial wavelengths of the other three media are 150 m, 120 m and 60 m, respectively.

Dip-Dependence of Stratigraphic and Evanescent Filtering

Both *stratigraphic filtering* and *evanescent filtering* cause high-frequency loss of seismic waves when they are reflected from a geologic structure beneath a sequence of sedimentary layers. The amount of high-frequency loss is determined by both the thickness of layers and the dip of the interface.

Figure 18 illustrates the geometry of zero-offset waves reflected from interfaces with different dips. The high-frequency loss of waves reflected from horizontal interfaces is only caused by stratigraphic filtering because no evanescent energy is produced, while this loss is mainly attributed to evanescent filtering for waves reflected from vertical interfaces because of their large propagation angles. As for an interface with a dip between 0° and 90°, the loss of high frequencies can be attributed to the

combined results of stratigraphic filtering and evanescent filtering. The stratigraphic filtering is weaker for steeper interfaces, as waves travel through less layers and spend more time in each layer; the filtering is the strongest for horizontal interfaces. On the contrary, the evanescent filtering is stronger for steeper interfaces, as waves travel at larger angles and produce more evanescent energy and faster decay. Reflections from a dipping interface have their high frequencies attenuated by the trade-off of the two filtering effects depending on the thickness of layers and the dip of the interface.

In Figure 3, I compared the frequency spectra of reflections from horizontal and vertical interfaces in an increasing-trend, velocity-layered medium with spatial wavelength comparable to the dominant wavelength of the seismic signal. The reflection from the vertical interface is dominated by low-frequency energy, while that from the horizontal interface is not. This observation demonstrates the strong evanescent filtering of seismic signals when the spatial wavelength of the medium is comparable to that of the seismic signal, while stratigraphic filtering is weak in this particular medium.

When the sedimentary layers of the medium get thinner, more high-frequency energy tunnels through high-velocity layers. However, shortening of the time-delay of short-period multiples increases the likelihood of losing high frequencies due to stratigraphic filtering. Therefore, the decrease in the thickness of layers decreases the high-frequency loss due to evanescent filtering but increases the loss due to stratigraphic filtering.

Figure 19 shows the scaled frequency spectra of waves reflected from different dipping interfaces with the same travel time, where the ratio of changes of the medium to that of the wavefield is less than 0.5. I use the frequency $f_{0.6}$, where the corresponding amplitude drops to 60% of the peak amplitude, to measure the frequency content of the reflection. The spectrum corresponding to the vertical interface contains more high frequencies than that for the horizontal interface; i.e., $f_{0.6}$ for the vertical interface is higher than $f_{0.6}$ for the horizontal interface. The $f_{0.6}$ for the 45° interface is higher than that for the horizontal interface, and lower than that for the vertical interface. This dip-dependent phenomenon tells us that the high-frequency loss of waves reflected from a dipping interface is dominated by stratigraphic filtering if the thickness of layers in the medium is much smaller than the seismic wavelength.

According to the above experiments and discussions, stratigraphic filtering is stronger with the decrease of reflector-dip or layer-thickness, while evanescent filtering is stronger with the increase of reflector-dip or layer-thickness. The high-frequency loss of waves reflected from a dipping interface is the combined result of the two filtering effects.
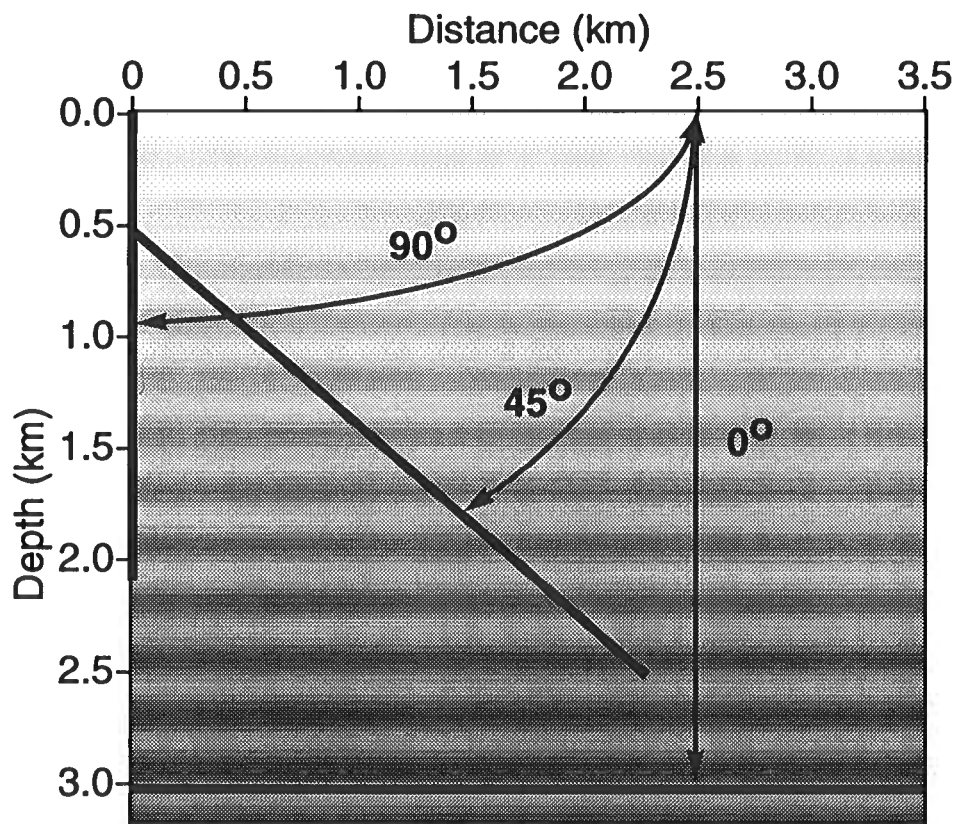
FIG. 18. Geometry of zero-offset reflections from interfaces with different dips. In a medium with a sequence of sedimentary layers, reflections from a steeper interface spend more time travelling in each layer.
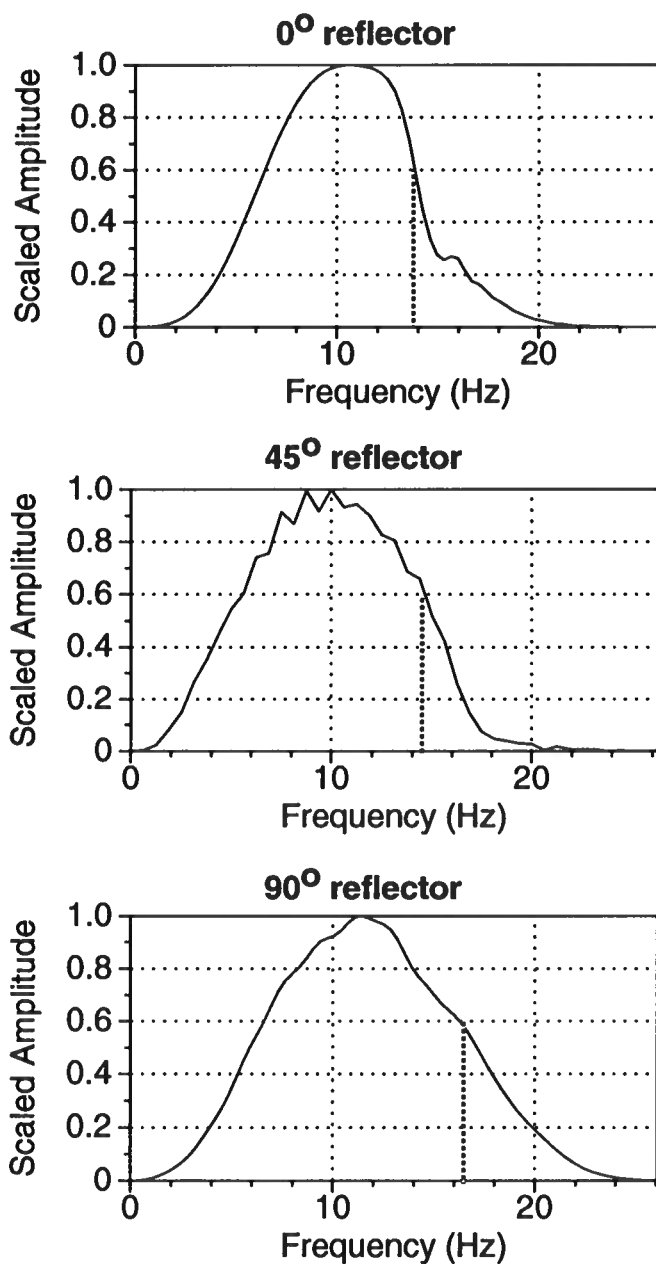
FIG. 19. Dip-dependent frequency distribution of zero-offset reflections with the same travel time. The velocity of the sedimentary medium has a linearly increasing trend of $1.6 + 0.5z$ (km/s), and a sinusoidal variation with a spatial wavelength of 60 m. The dominant frequency of source signal is 10 Hz. The dotted lines show frequencies which corresponding to 60% of peak amplitudes.

CONCLUSION

Summary

Seismic waves may lose their high frequencies, not only as a result of the inelasticity of media, but also as a result of the velocity layering when waves travel in a layered sedimentary sequence. Waves reflected from interfaces embedded in sedimentary media lose their high frequencies in a dip-dependent way.

Velocity layering may cause two possible low-pass filtering effects on reflection seismic waves: stratigraphic filtering and evanescent filtering. Both of these filtering effects depend on the dip of the reflecting interface. Stratigraphic filtering is caused by the destructive interference of short-period multiples; the steeper the reflector dip, the less high frequencies are lost due to the destructive interferences. Evanescent filtering is caused by repeated tunneling of the evanescent energy; the steeper the reflector dip, the more high frequencies are attenuated in high-velocity layers.

Stratigraphic and evanescent filtering of seismic waves are also affected by the thickness of layers in the medium. If the layers are thick relative to the seismic wavelength, waves reflected from a vertical interface are strongly affected by the evanescent filtering. The thicker the high-velocity layers are, the less high frequencies tunnel through these layers; hence, stronger evanescent filtering is applied to these waves. On the other hand, for waves reflected from a horizontal interface, the thicker the layers are, the less high frequencies are attenuated by the destructive interference of short-period multiples; hence, weaker stratigraphic filtering is applied to these waves. In Figure 20, we can see that the two filtering effects have the opposite dependence on the reflector dip and layer thickness.

Frequency content of waves reflected from a dipping interface beneath a layered medium is affected by the combined result of stratigraphic filtering and evanescent filtering. When the layers are thick relative to the seismic wavelength, the high-frequency loss is dominated by evanescent filtering; more and more high frequencies are lost with the increase of the reflector dip. However, when the layers are thin relative to the seismic wavelength, the high-frequency loss is dominated by stratigraphic filtering; less and less high frequencies are lost with the increase of the reflector dip.

The loss of high-frequency signals in seismic waves reflected from geologic structures due to velocity layering is important. Without those high frequencies, even a good migration technique will not be able to accurately image steep geologic structures. Better imaging of structures requires a dip-dependent deconvolution technique to regain those high frequencies.

Furthermore, horizontally traveling waves occur in cross-hole experiments as a rule rather than exception. Hence, the study of the attenuation of seismic waves due to velocity layering and large, non-vertical propagation angles may also be helpful for subsurface imaging in borehole-to-surface and borehole-to-borehole seismic surveys.

filtering		stratigraphic	evanescent
REFLECTOR	**steep**	weak	strong
	less steep	strong	weak
LAYERS	**thick**	weak	strong
	thin	strong	weak

FIG. 20. The dependence of stratigraphic filtering and evanescent filtering on the reflector dip and the layer thickness.

Suggestions for Future Research

Study of Reflections in Randomly-Layered Media

Statistical studies of the Earth's stratified lithology (e.g., Godfrey, 1980, Velzeboer, 1981, Banik et al., 1985b) show that a sedimentary sequence in the earth can be considered as a stochastic sequence, such as a Markov-chain. The Markov-chain approach yields synthetic sections similar to those recorded from cyclic deposits (e.g., Godfrey, 1980). Furthermore, Velzeboer (1981) noted that a major portion of the stratigraphical column of the Gulf of Mexico is made up of a binary sequence of sand and shale cyclic alternations. Quantitative studies on stratigraphic filtering have been conducted using these statistical sedimentary models (Godfrey et al. 1980, Banik et al. 1985a, 1985b, White et al. 1990). Banik (1985b) concluded that the effect of stratigraphic filtering on seismic waves depends on the statistical properties of the sedimentary sequence rather than the detail of the sediments.

However, the research in this thesis is based on a qualitative observation and analysis of the dip-dependent attenuation of synthetic seismograms. Reflections recorded in these seismograms correspond to increasing-trend, velocity-layered media. For a further study of this behavior, it is necessary to investigate whether evanescent filtering depends on the statistical properties of the medium, or on the detail of the sediments. Therefore stochastic-velocity background media are expected to be used in the study. In addition, a quantitative study is necessary for better understanding of evanescent filtering.

As inverse Q filtering is a reliable technique in compensating for the attenuation due to inelasticity, a good understanding of dip-dependent attenuation may lead to the possibility of developing a dip-dependent deconvolution technique which has a physical basis.

Improvement of Modeling Algorithm and Its Applications

Most methods for modeling waves reflected from complex structures, such as ray tracing and Kirchhoff modeling, assume that the background sedimentary medium is a smooth function, e.g., linearly increasing with depth. In contrast, the modeling algorithm described in this thesis can handle sedimentary media with fast variations with depth relative to seismic signals, e.g., increasing-trend, velocity-layered media. Therefore, this modeling method is useful for studying the behavior of seismic waves caused by velocity layering. However, the uniformly sampled grid is inefficient for the deep portion of the medium, which may have a much longer wavelength than does the shallow portion. An adjustable grid for finite-differencing, where the sampling spacing changes with the signal wavelength, may enhance the efficiency of the modeling.

This modeling method also has the advantage that it can handle complex geologic structures, as the only assumption made in the Born approximation is that of a small perturbation. Hence, theoretically, there are no restrictions on the shape of reflectors.

As the FKFD algorithm can be used to compute the Green function due to a 3-D point source, waves reflected from a 3-D geologic structure can be modeled using this same approach. However, the numerical representation of an arbitrary geometry of reflector is not trivial. Perhaps with the use of computational geometry techniques, geometry of reflectors can be better numerically represented, thus enhancing the ability of this modeling method to handle complex structures. In this 3-D case, the fast Hankel transform algorithm (Deng, 1991) can be used to compute, with an enhanced efficiency, waves reflected from a complicated 3-D geologic structure.

In addition to the study of dip-dependent attenuation of seismic waves, this modeling method can also be used to study other phenomena caused by thin layering or steeply dipping reflectors, such as thin density layering effects and transverse isotropy. This modeling may also be used for cross-hole tomography or amplitude-versus-offset (AVO) analysis.

Acknowledgments

References

Aki, K., Richards, P.G., 1980, Quantitative seismology, Theory and Methods: W.H. Freeman and Company.

Banik, I. L., Shuey, R.T., 1985a, Stratigraphic filtering, Part I: Derivation of the O'Doherty-Anstey formula: Geophysics **50**, 2768–2774.

Banik, I. L., Resnick, J.R. Shuey, R.T., 1985b, Stratigraphic filtering, Part II: Model spectra: Geophysics **50**, 2768–2774.

Bleistein, 1984, Mathematical methods for wave phenomena: Academic Press Inc.

Bleistein, N., Gray, S.H., 1985, An extension of the Born inversion method to a depth dependent reference profile: Geophysical Prospecting, **33** 999–1022.

Brown, David L., 1984, A note on the numerical solution of the wave equation with piecewise smooth coefficients: Mathematics of Computation **42**, 369–391.

Claerbout, J. F., 1985, Imaging the Earth's interior: Blackwell Scientific Publications.

Deng, H. L., 1991, Fast Hankel transform and its applications: **CWP-107**, Project Review, Colorado School of Mines.

Fuchs, K., Schulz, K., 1976, Tunneling of low-frequency waves through the subcrustal lithosphere: J. Geophysics **42**, 175–190.

Godfrey, R., Muir, F. Rocca, F., 1980, Modeling seismic impedance with Markov chains: J. Geophysics **45**, 1351–1372.

Korn, M., 1987, Computation of a wavefields in vertically inhomogeneous media by a frequency domain finite-difference method and application to wave propagation in earth models with random velocity and density perturbations: Geophysics J.R.astr.Soc. **88**, 345–377.

Larner, K., Beasley, C.J., Lynn, W., 1989, In quest of the flank: Geophysics **54**, 701–717.

O'Doherty, R.F., and Anstey, N.A., 1971, Reflections on amplitudes: Geophys. Prosp., **19**, 430-458.

Sochacki, J.S., George, J.H., Ewing, R.E., Smithson, S.B 1991, Interface conditions for acoustic and elastic wave propagation: Geophysics **56**, 168–181.

White, B., Sheng, P., Nair, B., 1990, Localization and backscattering spectrum of seismic waves in stratified lithology: Geophysics **55**, 1158–1165.

Velzeboer, C.J., 1981, The theoretical seismic reflection response of sedimentary sequences: Geophysics **46**, 843–853.

Yilmaz, Ö. , 1987, Seismic data processing: Society of Exploration Geophysics.

Appendix A

DERIVATION OF FINITE-DIFFERENCE EQUATIONS

The finite-differencing for obtaining the frequency-wavenumber response of a layered medium starts from the equation,

$$\rho \frac{d}{dz}\frac{1}{\rho}\frac{d}{dz}P + \left(\frac{\omega^2}{v^2(z)} - k^2\right)P = -\frac{\omega^2}{v^2(z)}\delta(z - z_s)S(\omega), \tag{A-1}$$

where $S(\omega)$ is the Fourier transformed signature of a source at depth z_s and $P(\omega, k, z)$ is the pressure field. The frequency and wavenumber response in equation (A-1) is solved by a finite-difference scheme known as the "1/6 trick" (e.g., Claerbout, 1985).

For a uniformly sampled grid, the medium is discretized into a set of thin "layers", which have the same thicknesses. In each "layer", the velocity and density functions are assumed to be smooth. The derivative of density in equation (A-1) requires the interpolation of density between grid points; therefore the first term in equation (A-1) is discretized by introducing fictitious grid points in the middle of the "layers" to perform two successive differences. As shown in Figure A-1, grid points are sampled at the interfaces of the "layers" and the two fictitious points are in the middle of the "layers". The second-order differential operator in equation (A-1) is performed centered on the real and fictitious grid points successively; this term is approximated by

$$
\begin{aligned}
\frac{\delta}{\delta z}\frac{1}{\rho}\frac{\delta}{\delta z}P &= \frac{1}{\Delta z}\frac{\delta}{\delta z}\left[\frac{1}{\rho_z}\left(P_{z+1/2} - P_{z-1/2}\right)\right] \\
&= \frac{1}{\Delta z^2}\left[\frac{1}{\rho_{z+1/2}}P_{z+1} - \left(\frac{1}{\rho_{z+1/2}} + \frac{1}{\rho_{z-1/2}}\right)P_z + \frac{1}{\rho_{z-1/2}}P_{z-1}\right].
\end{aligned} \tag{A-2}
$$

I have assumed that the reciprocal of the density function is piecewise linear; hence, the reciprocal of the density at depth z is

$$\frac{1}{\rho(z)} = \frac{1}{\rho_i} + \left(\frac{1}{\rho_i} - \frac{1}{\rho_{i+1}}\right)\frac{z - z_i}{\Delta z}, \tag{A-3}$$

where $z_i < z < z_{i+1}$ and ρ_i is the density of the ith grid point at depth z_i. Therefore, the densities at fictitious grid points are

$$\frac{1}{\rho_{z-1/2}} = \frac{1}{2}\left(\frac{1}{\rho_{z-1}} + \frac{1}{\rho_z}\right),$$

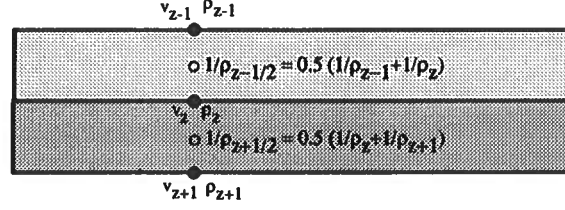$$\frac{1}{\rho_{z+1/2}} = \frac{1}{2}\left(\frac{1}{\rho_z} + \frac{1}{\rho_{z+1}}\right). \tag{A-4}$$

FIG. A-1. The discretized model of a vertically stratigraphic medium in the finite-differencing.

The "1/6 trick" finite-difference scheme approximates a second-order differential operator as

$$\frac{d^2}{dz^2} \approx \frac{\frac{\delta^2}{\delta z^2}}{1 + \gamma \Delta^2 \frac{\delta^2}{\delta z^2}}, \tag{A-5}$$

where γ is an adjustable constant (e.g., Claerbout, 1985). $\gamma = 0$ is equivalent to the standard second-order approximation. Using this second-order finite-difference scheme, equation (A-1) is approximated by

$$\rho \frac{\delta}{\delta z} \frac{1}{\rho} \frac{\delta}{\delta z} P + (\frac{\omega^2}{v^2} - k^2)(1 + \gamma \Delta z^2 \frac{\delta^2}{\delta z^2})P = -\frac{\omega^2}{v^2}(1 + \gamma \Delta z^2 \frac{\delta^2}{\delta z^2})S(\omega, z), \tag{A-6}$$

where $S(\omega, z) = S(\omega)\delta(z - z_s)$. The first term in equation (A-6) is represented by equation (A-2) and the other second-order difference operator is represented by

$$\frac{\delta^2}{\delta z^2} P = \frac{1}{\Delta z^2} (P_{z+1} - 2P_z + P_{z-1}). \tag{A-7}$$

After the discretization, the differential equation is reduced to a tri-diagonal linear system. This tri-diagonal linear system, the approximation of equation (A-1), is given by

$$\begin{bmatrix} b_0 & c_0 & 0 & \cdots & 0 \\ a_1 & b_1 & c_1 & 0 & \cdots \\ 0 & a_2 & b_2 & c_2 & \cdots \\ \vdots & 0 & \ddots & \ddots & \ddots \\ 0 & \vdots & \vdots & a_{n-1} & b_{n-1} \end{bmatrix} \begin{bmatrix} P_0 \\ P_1 \\ \vdots \\ P_{n-2} \\ P_{n-1} \end{bmatrix} = \begin{bmatrix} d_0 \\ d_1 \\ \vdots \\ d_{n-2} \\ d_{n-1} \end{bmatrix}, \tag{A-8}$$

where the coefficients are

$$
\begin{aligned}
a_i &= \frac{\rho_i}{\Delta z^2}\frac{1}{\rho_{i-1/2}} + \gamma(\frac{\omega^2}{v_i^2} - k^2), \\
b_i &= -\frac{\rho_i}{\Delta z^2}(\frac{1}{\rho_{i+1/2}} + \frac{1}{\rho_{i-1/2}}) + (1 - 2\gamma)(\frac{\omega^2}{v_i^2} - k^2), \\
c_i &= \frac{\rho_i}{\Delta z^2}\frac{1}{\rho_{i+1/2}} + \gamma(\frac{\omega^2}{v_i^2} - k^2), \\
d_i &= -\frac{\omega^2}{v_i^2}\left[\gamma S_{i+1} + (1 - 2\gamma)S_i + \gamma S_{i-1}\right], \\
i &= 1, \cdots, n - 2,
\end{aligned}
\tag{A-9}
$$

where n is the number of samples in depth. The tri-diagonal system equation (A-8) can be solved by standard techniques (e.g., Claerbout, 1985, 99).

The surface boundary is assumed to be *absorbing*, that is, the waves reaching the surface of the model continue to propagate into an upper half-space without being reflected from the surface. Therefore, no surface multiples are produced at an absorbing surface and only up-going waves exist in the medium above the surface. As the same boundary condition applies to the bottom of the medium, only down-going waves propagate into the lower half-space. Hence, the waves reaching the boundaries are represented by

$$
\begin{aligned}
p(\omega, k, z) &= p(\omega, k, z - \Delta z)e^{ik_z \Delta z}, && \text{for} && z > z_{max}; \\
p(\omega, k, z) &= p(\omega, k, z + \Delta z)e^{ik_z \Delta z}, && \text{for} && z < z_{min};
\end{aligned}
$$

$$
\text{where} \qquad k_z = \sqrt{\frac{\omega^2}{v^2} - k^2}.
\tag{A-10}
$$

In the tri-diagonal linear system equation (A-8), the boundary coefficients are given by

$$
\begin{aligned}
b_0 &= b_1 + a_1 e^{ik_z \Delta z}, \\
c_0 &= c_1, \\
d_0 &= \begin{cases} -\frac{\omega^2}{v_0^2}S(\omega), & \text{if } z_s = z_{min}; \\ 0, & \text{otherwise}. \end{cases} \\
b_{n-1} &= b_{n-2} + c_{n-2} e^{ik_z \Delta z}, \\
a_{n-1} &= a_{n-2}, \\
d_{n-1} &= \begin{cases} -\frac{\omega^2}{v_{n-1}^2}S(\omega), & \text{if } z_s = z_{max}; \\ 0, & \text{otherwise}. \end{cases}
\end{aligned}
$$

(A-11)

(A-12)

In the finite-difference approximation described above, γ is an adjustable constant for reducing the approximation error; $\gamma = 1/12$ is used throughout this thesis. The accuracy of this finite-difference approach is discussed in Appendix B.

Appendix B

ACCURACY OF FINITE-DIFFERENCE APPROXIMATION

Finite-difference approximations are well known for causing numerical dispersion and anisotropy. Referring to equation (A-1), a vertical wavenumber quantity k_z can be defined as,

$$k_z^2 \equiv \frac{\omega^2}{v^2} - k^2. \tag{B-1}$$

From the finite-difference scheme described in Appendix A, a numerical approximation $\hat{k}_z$ for k_z can be estimated. The phase-velocity c of waves computed from the numerical scheme is a function of both frequency and propagation angle. This phase-velocity is related to the horizontal wavenumber k and the approximation to the vertical wavenumber $\hat{k}_z$ by

$$\hat{k}_z^{\;2} + k^2 = \frac{\omega^2}{c^2}, \tag{B-2}$$

showing that the phase-velocity c differs from the true velocity function of the medium v because of the approximations to differential operators.

Using the approximation to a second-order differential operator in equation (A-5), the accuracy can be estimated by (e.g., Claerbout, 1985)

$$
\begin{aligned}
\hat{k}_z &= \frac{2\sin\frac{k_z\Delta z}{2}}{\sqrt{1 - 4\gamma\sin^2\frac{k_z\Delta z}{2}}} \\
&= k_z\left(1 + \frac{12\gamma - 1}{24}k_z^2\Delta z^2 + \frac{1 - 120\gamma + 720\gamma^2}{1920}k_z^4\Delta z^4 + O(k_z^6\Delta z^6)\right).
\end{aligned}
\tag{B-3}
$$

Fourth-order accuracy is achieved when γ is set to be $1/12$,

$$\hat{k}_z = k_z\left(1 - \frac{1}{480}k_z^4\Delta z^4 + O(k_z^6\Delta z^6)\right). \tag{B-4}$$

The accuracy of the approximations for $\gamma = 0, 1/12$ are shown in Figure B-1. It can be seen that the "1/6 trick", with $\gamma = 1/12$, is a better approximation to a second-order operator than is the ordinary second-order approximation.

Numerical dispersion and anisotropy caused by a finite-difference approximation is represented by the frequency- and propagation-angle-dependent phase-velocity. If θ is the propagation angle of waves in respect to the vertical, from equation (B-1) we have,

$$k_z = \frac{\omega}{v}\cos\theta,$$
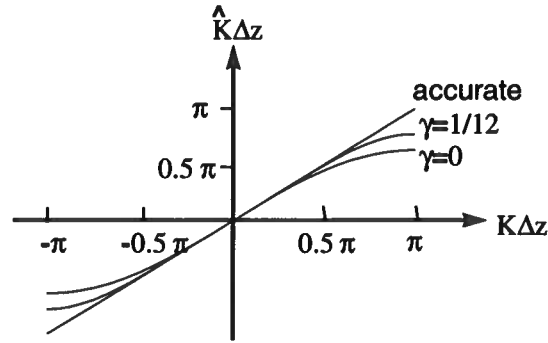
$$k = \frac{\omega}{v}\sin\theta. \tag{B-5}$$

FIG. B-1. The increase of the accuracy in the finite-difference modified second-order approximation with $\gamma = 1/12$. $\gamma = 0$ is the ordinary second-order finite-difference approximation.

Substituting equation (B-5) into equations (B-2) and (B-4), the numerical phase velocity is

$$c(\theta, \omega) \approx \frac{v}{\sqrt{\left|1 - \frac{\cos^6\theta}{240} \frac{\omega^4 \Delta z^4}{v^4}\right|}}. \tag{B-6}$$

In equation (B-6),

$$1 - \frac{\cos^6\theta}{240} \frac{\omega^4 \Delta z^4}{v^4} \geq 0 \tag{B-7}$$

since the depth sampling spacing Δz has to satisfy the sampling theorem:

$$\Delta z \leq \frac{\pi}{k_z} = \frac{\pi v}{\omega \cos\theta}. \tag{B-8}$$

It can be seen that the phase velocity error decreases as the propagation angle increases or frequency decreases. The numerical error at the maximum frequency is the most significant, and horizontal traveling waves have the best accuracy.